

# OpenGround: Active Cognition-based Reasoning for Open-World 3D Visual Grounding

Wenyuan Huang<sup>◊</sup> Zhao Wang<sup>△</sup> Zhou Wei<sup>△</sup> Ting Huang<sup>◊</sup>

Fang Zhao<sup>◊</sup> Jian Yang<sup>◊</sup> Zhenyu Zhang<sup>◊, ✉</sup>

<sup>◊</sup>Nanjing University, School of Intelligent Science and Technology

<sup>△</sup>China Mobile Zijin Innovation Institute

## Abstract

3D visual grounding aims to locate objects based on natural language descriptions in 3D scenes. Existing methods rely on a pre-defined Object Lookup Table (OLT) to query Visual Language Models (VLMs) for reasoning about object locations, which limits the applications in scenarios with undefined or unforeseen targets. To address this problem, we present OpenGround, a novel zero-shot framework for open-world 3D visual grounding. Central to OpenGround is the Active Cognition-based Reasoning (ACR) module, which is designed to overcome the fundamental limitation of pre-defined OLTs by progressively augmenting the cognitive scope of VLMs. The ACR module performs human-like perception of the target via a cognitive task chain and actively reasons about contextually relevant objects, thereby extending VLM cognition through a dynamically updated OLT. This allows OpenGround to function with both pre-defined and open-world categories. We also propose a new dataset named OpenTarget, which contains over 7000 object-description pairs to evaluate our method in open-world scenarios. Extensive experiments demonstrate that OpenGround achieves competitive performance on Nr3D, state-of-the-art on ScanRefer, and delivers a substantial 17.6% improvement on OpenTarget.

## 1. Introduction

3D Visual Grounding (3DVG) aims to locate target objects in 3D scenes from natural language descriptions, with broad applications in AR/VR systems [6, 34, 53, 68], vision-language navigation [12, 16, 69] and intelligent robot environmental perception [7, 21, 31]. An effective and applicable 3DVG approach should not only understand and reason over natural language descriptions but also flexibly adapt to targets of different granularities, from coarse object categories to fine-grained parts, and generalize to diverse and previously unseen environments in the real world.

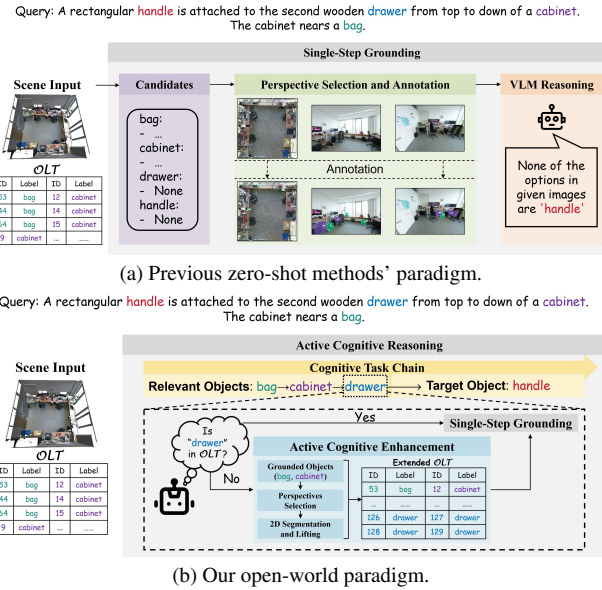


Figure 1. Comparative overview of previous zero-shot methods’ paradigm and ours. Previous paradigm is single-step grounding based on predefined OLT, unable to ground undefined objects. In contrast, our method introduces Active Cognition-based Reasoning to the paradigm, which enhances cognition before each grounding step and grounds target object progressively.

Current research in 3DVG has made significant progress, encompassing both supervised and zero-shot methods. While supervised methods [10, 13, 15, 23, 26, 38, 71, 76], trained on diverse datasets [1, 4, 6, 9, 47, 67], achieve high accuracy on existing benchmarks, their generalization is inherently constrained by the object-level domains of current datasets. These datasets typically contain isolated object instances with limited category diversity, which leads such models to struggle when encountering novel or undefined fine-grained objects in real-world scenes. To improve the generalization of 3DVG methods, several zero-shot approaches [24, 25, 33, 46, 59, 65, 74] have been proposed,

leveraging the capabilities of 2D Vision-Language Models (VLMs) [3, 37, 55]. These approaches primarily follow the paradigm illustrated in Fig. 1: they first identify potential candidates from a pre-defined Object Lookup Table ( $\mathcal{OLT}$ ), subsequently determine appropriate viewpoints to inspect these candidates, and ultimately assign ID/bbox annotations to the candidates in the selected viewpoints before querying the VLM to confirm the target object’s ID. However, the main problem of these methods is also significant: they heavily depend on the  $\mathcal{OLT}$ , and thus fail to ground objects that have not been pre-defined. Actually, many open-world scenarios, such as cluttered offices, industrial environments, or rooms freshly reconstructed online, are filled with a multitude of small or unforeseen objects. Exhaustively pre-defining all such categories is impractical and computationally prohibitive. Consequently, extending the current VLM-based approaches to function effectively in such open-world scenarios, becomes a problem of paramount importance.

In this paper, we propose OpenGround, a novel zero-shot framework that supports open-world 3D visual grounding while remaining compatible with existing zero-shot methods. As illustrated in Fig. 1, OpenGround introduces Active Cognition-based Reasoning (ACR) module to adapt the 3DVG pipeline to undefined objects. The core idea is enhancing the cognition of VLMs on the open-world scenes by human-like cognitive planning and active contextual perception. ACR first builds a cognitive task chain according to the given description based on VLM reasoning. Such a task chain decomposes the objective into a structured sequence of grounding actions for relevant objects, emulating human spatial reasoning. Based on the sequence, ACR introduces Active Cognition Enhancement (ACE) module to actively perceive and reason about the next relevant object by leveraging the context of previously grounded ones under a progressive criterion, subsequently enhancing the cognition of VLMs with a continuously updated  $\mathcal{OLT}$ . In this way, OpenGround efficiently grounds the undefined 3D targets, breaking through the limitation of pre-defined  $\mathcal{OLT}$  in open-world scenarios.

To evaluate our framework, we also construct a novel dataset named OpenTarget. The dataset takes ScanNet++ [63] as the basement, and integrate fine-grained part-level segmentation results from Articulate3D [11] as the targeted but undefined 3D objects to simulate the open-world setting. With the automatic description generating and rigorous quality filtering, we obtain 7,724 query-object pairs which are sufficiently comprehensive to support reliable validation experiments. Overall, our contributions are summarized as follows:

- We define a novel task for zero-shot 3DVG: grounding objects outside the predefined object lookup table ( $\mathcal{OLT}$ ) in 3D environments using natural language descriptions. We further propose a benchmark named OpenTarget to

enable rigorous evaluation of the open-world 3DVG task. The dataset uses VLM-generated natural language descriptions, and ensures final quality through manual filtering, resulting in 7,724 high-quality query-object pairs.

- We extend the existing zero-shot 3DVG paradigm by integrating the Active Cognition Enhancement (ACE) module, which enables the framework to ground objects beyond the  $\mathcal{OLT}$ .
- We propose a human-like task chain reasoning mechanism for progressive grounding. The mechanism restricts ACE application to regions around already grounded reference objects, balancing computational efficiency and contextual grounding precision.

## 2. Related Work

**Supervised 3DVG.** Supervised 3D visual grounding began with ScanRefer [6] and Referit3D [1], and can be categorized into two paradigms: two-stage and single-stage methods. Two-stage approaches [1, 6, 17, 23, 67, 70, 75] first generate object proposals via 3D detection or segmentation [18, 32, 44, 54], then match them to textual queries. In contrast, single-stage methods [10, 13, 15, 26, 38, 39, 52, 57, 71] employ end-to-end architectures that jointly learn 3D and language representations for direct localization. Recent advances [15, 38, 60, 73] further integrate LLMs or VLMs to enhance 3D understanding, forming specialized 3D-VLMs. Despite their success, particularly 3D-R1 [15] which achieves state-of-the-art results through large-scale GRPO [45] training, these methods remain limited by their training datasets and fail to generalize to open-world or part-level grounding, as in our OpenTarget dataset.

**Zero-Shot 3DVG.** Zero-shot 3DVG aims to overcome the limited generalization of supervised methods by leveraging VLMs’ reasoning and cross-modal understanding. Existing works fall into two paradigms: LLM-based and VLM-based. LLM-based approaches [61, 64, 65] convert 3D scenes into text and use LLMs with external tools (*e.g.*, visual programs, spatial reasoning) for grounding, benefiting from strong reasoning but lacking fine visual cues such as color or texture. VLM-based methods [19, 24, 25, 59, 66, 74] integrate textual and visual features for more precise localization. Although achieving near-supervised performance, most rely on a predefined object lookup table ( $\mathcal{OLT}$ ), limiting open-world grounding. VLM-Grounder [59] attempts to remove this dependency, but still struggles with insufficient observation and limited cognition for novel objects in open-world scenarios.

**Advances in VLMs and Visual Perception.** Recent VLMs [2, 3, 8, 27–29, 49–51, 55, 56], such as GLM-4.5V, the Qwen-VL, and InternVL series, show strong cross-domain generalization and fine-grained spatial understanding [49, 56]. Meanwhile, 3D perception frameworks like Point-Group [18], Mask3D [44], and Point-SAM [72] have ad-

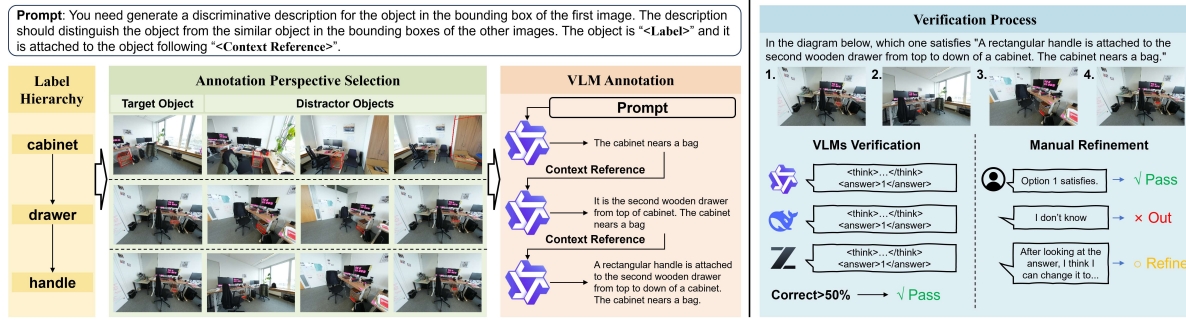


Figure 2. **Data Collection Pipeline.** The pipeline generates discriminative object descriptions via three annotation stages and two-stage verification. It leverages hierarchical labels (*e.g.*, cabinet→drawer→handle), selects target–distractor views, and employs VLMs for context-aware descriptions using parent annotations. Quality is ensured via VLM voting and manual refinement.

vanced but still lack open-domain generalization due to limited 3D data. In contrast, 2D foundation models such as SAM [20, 41], GroundingDINO [30], GroundedSAM [43], and DEIMv2 [14] achieve strong open-world segmentation and grounding. The convergence of spatially aware VLMs and generalizable 2D perception models makes open-world 3D object grounding both feasible and promising.

### 3. Dataset

To rigorously evaluate the open-world grounding capability of our OpenGround framework, we construct a novel dataset named OpenTarget, based on ScanNet++ [63] and Articulate3D [11]. Existing 3DVG benchmarks [1, 6] focus on object-level instances with limited category diversity, failing to simulate the open-world scenarios where fine-grained, previously undefined objects (*e.g.*, sink handles, cabinet doors) are pervasive. In contrast, OpenTarget introduces objects from Articulate3D that are absent from the object lookup table ( $\mathcal{OLT}$ ) built on ScanNet++. These fine-grained parts mimic unforeseen objects in open-world scenarios, providing a realistic benchmark for open-world grounding. OpenTarget provides totally 7,724 object-pairs for segments in Articulate3D, across 120 class labels - 50 object classes and 70 part classes. We outline the dataset construction below and statistics in the **Appendix**.

**Annotation.** As illustrated in Fig. 2, we adopt a progressive VLM-based strategy for annotation, involving three stages: Label Hierarchy, Annotation Perspective Selection, and VLM Annotation. First, we utilize the hierarchical labels from Articulate3D (*e.g.*, cabinet→drawer→handle), starting from top-level objects in subsequent processes. Second, we collect the target and its distractors, and select suitable perspectives for each. Third, we prompt VLMs with these perspectives and labels to generate discriminative descriptions that distinguish the target from distractors. For child objects, we repeat the process with parent object annotations as contextual references, ensuring progressively de-

tailed and discriminative descriptions.

**Verification.** We employ a two-stage quality verification process, combining automatic filtering and manual refinement. First, for objects with the same label, we use multiple VLMs to vote on object-query pairs (via selected perspectives and object IDs), retaining only majority-approved pairs to manual review. Subsequently, human annotators verify these pairs, with the ability to mark them as “unidentifiable” or revise queries, ensuring high dataset quality.

### 4. Methodology

**Overview.** Zero-shot 3D Visual Grounding (3DVG) methods take a 3D scene  $\mathcal{S}$ , a language query  $\mathcal{Q}$ , and an Object Lookup Table ( $\mathcal{OLT}$ ) as inputs. The  $\mathcal{OLT}$  maps object IDs to their semantic labels and 3D bounding boxes:

$$\mathcal{OLT} = \{(\mathbf{ID}_i, \mathbf{label}_i, \mathbf{bbox}_i) \mid i = 1, 2, \dots, N\}. \quad (1)$$

A 3D scene  $\mathcal{S}$  consists of a point cloud  $\mathcal{P}$ , RGB observations  $\mathcal{I} = \{\mathbf{I}_k\}_{k=1}^K$ , and camera parameters  $(\mathbf{R}_k, \mathbf{T}_k)$ , providing multi-view visual information for grounding. These methods locate the target’s  $\mathbf{bbox}$  by matching  $\mathcal{Q}$  to entries in  $\mathcal{OLT}$ , but are restricted to known objects within the table. Our OpenGround framework overcomes this by enabling open-world grounding, allowing localization of both known and novel objects beyond  $\mathcal{OLT}$ .

As illustrated in Fig. 3, the Active Cognition-based Reasoning (ACR) module is the core of our framework, executing progressive open-world 3D grounding via three sub-modules. First, the Cognitive Task Chain Construction module (Sec. 4.1) parses the query into target and relevant objects using the VLM, retrieves  $\mathcal{OLT}$  candidates via semantic similarity, and constructs a sequential task chain to guide step-by-step grounding. Next, ACR grounds objects along the task chain. For objects absent from the initial  $\mathcal{OLT}$ , the Active Cognition Enhancement module (Sec. 4.2) selects perspectives around previously grounded objects, performs 2D segmentation and lifts results to 3D to

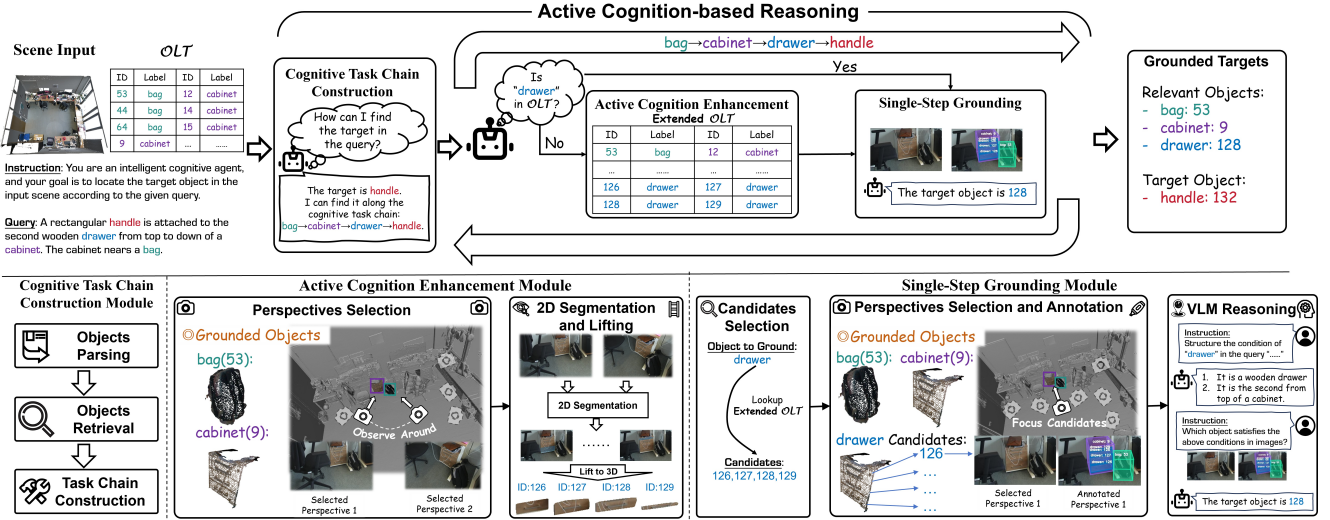


**Figure 3. Overview of the OpenGround framework.** The core of our framework is the Active Cognition-based Reasoning (ACR) module. First, the ACR invokes Cognitive Task Chain Construction module to obtain a sequential task chain to guide step-by-step grounding. Next, the ACR module progresses along the task chain to ground objects progressively. For objects not present in the  $OLT$ , it activates the Active Cognition Enhancement module to extend the  $OLT$  with newly perceived objects around previously grounded objects. Then, the ACR module uses Single-Step Grounding which prompts VLM with annotated images from perspectives focused on candidates (with reference to previously grounded objects) to obtain the target object's ID in this step. The ID is used to retrieve the object's 3D bounding box from the extended  $OLT$ . Upon completing the ACR module's workflow, we obtain the bounding box of the final target.

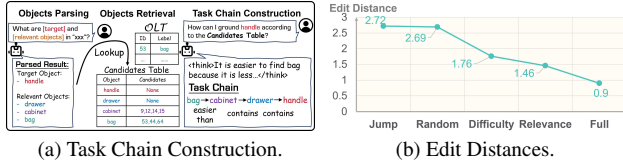


**Figure 4.** (a) illustrates three sequential steps (Objects Parsing, Objects Retrieval, Task Chain Construction) and contrasts human-like reasoning. (b) shows the edit distances between constructed and human given task chains.

extend the  $OLT$ . Then, the Single-Step Grounding module (Sec. 4.3) follows existing paradigm with an adaption: it incorporates previously grounded objects into perspectives selection, then leverages the VLM to obtain the target's ID for 3D bbox retrieval from the extended  $OLT$ . Through task chain iteration, ACR completes grounding of all query-relevant objects and outputs the final target's 3D bbox, no matter within or beyond the initial  $OLT$ .

#### 4.1. Cognitive Task Chain Construction

Human object grounding relies on sequential and context-dependent cognition, and rarely locates a target without first identifying its surrounding context: to find a “drawer handle”, we first locate the “drawer” and then the “handle” belongs to the drawer. Existing 3DVG methods, however,

match queries to  $OLT$  entries in a single step, ignoring hierarchical context and often failing in tasks with multiple relevant objects. To address this, we propose the Cognitive Task Chain Construction module, which emulates human cognitive planning by decomposing complex grounding into an ordered sequence of sub-tasks (each grounding a context object to inform the next), as shown in Fig. 4a. **Objects Parsing.** We input the query  $Q$  into a VLM to extract two core components: the target object label  $L^{tgt}$  and a set of relevant objects' labels  $\{L_j^{rel}\}_{j=1}^n$ . Formally the parsing process is expressed as:

$$(L^{tgt}, \{L_j^{rel}\}_{j=1}^n) = \text{VLM}(Q). \quad (2)$$

**Objects Retrieval.** For each parsed object label  $L_j \in \mathcal{L} = \{L_j^{rel}\}_{j=1}^n \cup \{L^{tgt}\}$ , we retrieve candidate object IDs from the initial  $OLT$  via text similarity matching. Formally, the candidate ID set  $\mathcal{C}_j$  for label  $L_j$  is defined as:

$$\mathcal{C}_j = \left\{ \text{ID}_i \mid \frac{E_{L_j} \cdot E_{\text{label}_i}}{\|E_{L_j}\| \cdot \|E_{\text{label}_i}\|} \geq \tau_{cand}, \text{ID}_i \in OLT \right\}, \quad (3)$$

where  $E_{L_j}$  and  $E_{\text{label}_i}$  are the embedding of the label  $L_j$  and  $\text{label}_i$ ,  $\tau_{cand}$  is the threshold to accept the candidate.

**Task Chain Construction.** Human cognitive planning for object grounding balances semantic relevance and task difficulty. To emulate this, we prompt the VLM with parsed object labels and their candidate set sizes (seen as difficulty

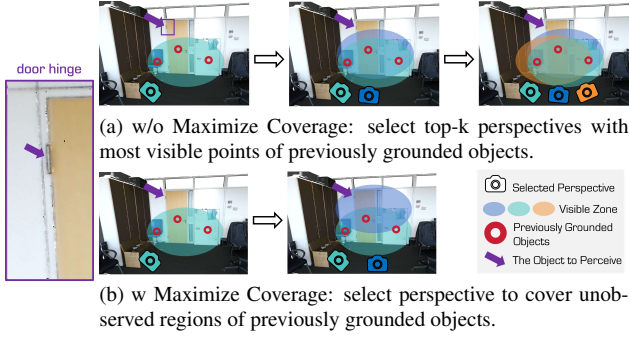


Figure 5. Illustration of perspective selection strategies in ACE.

in Nr3D [1]) to generate the ordered indices of  $\mathcal{L}$  as the Cognitive Task Chain  $\mathcal{T}$ :

$$\mathcal{T} = \text{VLM}(\mathcal{Q}, \mathcal{L}, \{\|\mathcal{C}_j\| \mid j \in [1, n+1]\}), \quad (4)$$

where  $\mathcal{T} = [T_1, T_2, \dots, T_{n+1}]$  with  $T_{n+1} = n+1$  (ensuring the target is the last one). To validate human alignment, we compare  $\mathcal{T}$  with human-constructed ones from a user questionnaire, using the weighted average edit distance [22, 35], which measures structural similarity between two sequences. We evaluate several strategies: **Full** is the proposed strategy; **Relevant**: sorting by relation to the target object via  $\mathcal{T} = \text{VLM}(\mathcal{Q}, \mathcal{L})$ ; **Difficulty**: sorting by candidate set size, and randomizing the objects without candidates; **Random**: randomly sorting; **Jump**: adopting the first and last objects from **Full** results (localizing one reference, then targeting directly). As shown in Fig. 4b, our **Full** strategy achieves the lowest distance, indicating the closest alignment with human reasoning. Considering the diversity of human-constructed task chains, this consistently low edit distance demonstrates that our method captures the shared patterns of human cognitive planning, exhibiting human-like reasoning and task ordering.

## 4.2. Active Cognition Enhancement

During open-world object grounding, encountering objects out-of- $\mathcal{OLT}$  is inevitable. However, existing methods rely on a pre-defined, static  $\mathcal{OLT}$  that remains unchanged throughout grounding, resulting in fixed and limited scene cognition that fails in open-world scenarios. To address this, we propose the Active Cognition Enhancement module, which actively perceives novel objects and enhances scene cognition via extending the  $\mathcal{OLT}$  when an object is not found within it, enabling open-world grounding and promising the compatibility with existing methods.

**Perspectives Selection.** To actively perceive novel objects efficiently in the current task  $T_t$ , we select observation perspectives  $\mathcal{I}^*$ , from the full images set  $\mathcal{I}$ , around previously grounded objects  $[O_1, \dots, O_{t-1}]$  from prior tasks  $[T_1, \dots, T_t]$ . The selected perspectives  $\mathcal{I}^*$  should maximize coverage of previously grounded objects, instead of

only focusing on their most visible points, as illustrated in Fig. 8. Thus, we perform a greedy strategy to select  $V$  perspectives at most, to ensure sufficient observation of grounded objects while reducing computational overhead in subsequent processes. For each object  $O_i$ , we initialize its observed regions as  $\mathcal{R}_{O_i}^0 = \emptyset$  which will be added with observed points of the object. Then, we incrementally add perspectives from  $v = 1$  to  $V$ . For each candidate view  $k$ , its coverage gain is defined as follows:

$$\Delta(k) = \sum_{O_i} \frac{|\mathcal{P}_{O_i} \cap \mathcal{P}_k \setminus \mathcal{R}_{O_i}^{v-1}|}{|\mathcal{P}_{O_i}|}, \quad (5)$$

where  $\mathcal{P}_{O_i}$  is the point set of object  $O_i$ ,  $\mathcal{P}_k$  denotes the 3D points visible from view  $k$ , and  $\mathcal{R}_{O_i}^{v-1}$  denotes the observed region of  $O_i$  after  $v-1$  perspectives have been selected. At each step  $v$ , we select the best candidate view  $k^*$  that maximizes  $\Delta(k^*)$ , add the image  $\mathbf{I}_{k^*}$  into  $\mathcal{I}^*$ , and update

$$\mathcal{R}_{O_i}^v = \mathcal{R}_{O_i}^{v-1} \cup (\mathcal{P}_{O_i} \cap \mathcal{P}_{k^*}), \forall O_i. \quad (6)$$

This process continues until all previously grounded objects are fully observed (*i.e.*,  $\mathcal{R}_{O_i}^v = \mathcal{P}_{O_i}, \forall O_i$ ) or the maximum number of perspectives  $V$  is reached. Finally, the resulting  $\mathcal{I}^*$  serves as the optimized observation perspectives, ensuring sufficient coverage of grounded objects while reducing redundant information and computational overhead.

**2D Segmentation and Lifting.** Once the observation perspectives  $\mathcal{I}^*$  are selected, the next step is to perceive the novel object in each view and lift it to 3D to extend the  $\mathcal{OLT}$ . For each RGB image  $\mathbf{I}_k \in \mathcal{I}^*$ , we perform 2D segmentation to identify candidate regions that may correspond to the object. Formally, let  $\mathcal{M}_k = \text{SEG}(\mathbf{I}_k, L_{T_t})$  denote the set of segmented masks in view  $k$ , where **SEG** is any open-vocabulary 2D segmentation model. Then the 2D masks are lifted into 3D using corresponding point clouds  $\mathcal{P}_k$ . For each mask  $m \in \mathcal{M}_k$ , the lifted 3D points are:

$$\mathcal{P}_m = \{\mathbf{p} \in \mathcal{P}_k \mid \mathbf{p} \text{ projects inside mask } m \text{ in view } k\}. \quad (7)$$

All the lifted 3D masks from all views in  $\mathcal{I}^*$  are then aggregated into a single set  $\{\mathcal{P}_m \mid m \in \mathcal{M}_k, \forall k\}$ . Following the practice in Open3DIS [36], we iteratively merge masks whose 3D point sets have high spatial overlap, measured by their IoU. Specifically, two masks  $\mathcal{P}_{m_i}$  and  $\mathcal{P}_{m_j}$  are merged if  $\text{IoU}(\mathcal{P}_{m_i}, \mathcal{P}_{m_j}) \geq \tau_{iou}$  where  $\tau_{iou}$  is a predefined threshold. The merging process continues until no further pairs satisfy the condition. After convergence, we obtain a set of distinct 3D masks  $\{\mathcal{P}_1, \mathcal{P}_2, \dots, \mathcal{P}_M\}$ . To improve robustness, we apply noise filtering to remove sparse outliers on each of the set. Finally, these 3D masks are added to the  $\mathcal{OLT}$  as new entries:

$$\mathcal{OLT} \leftarrow \mathcal{OLT} \cup \{(\text{ID}(i), L_{T_t}, \text{bbox}(\mathcal{P}_i)) \mid i \in [1, M]\}, \quad (8)$$

where  $\mathbf{ID}(i)$  denotes next unique id and  $\text{bbox}(\mathcal{P}_i)$  is the bounding box of  $\mathcal{P}_i$ . This process enhances scene cognition of novel objects and enables OpenGround to continuously enrich the  $\mathcal{OLT}$  with novel objects actively perceived.

### 4.3. Single-Step Grounding

After cognition enhancement, the extended  $\mathcal{OLT}$  supports grounding of objects beyond the initial  $\mathcal{OLT}$ . We build on existing single-step paradigms with a key adaptation for our cognitive task chain: rather than treating each grounding instance independently, we leverage previously grounded objects as contextual references for the current task. This preserves existing core logic while boosting accuracy via contextual constraints, with detailed steps as follows.

**Candidates Selection.** Similar to the Sec. 4.1, the grounding process first retrieves a set of candidate objects from the extended  $\mathcal{OLT}$ . This step ensures that grounding is conducted only within a contextually relevant subset of objects, effectively narrowing the search space.

**Perspectives Selection and Annotation.** For each candidate object  $c_i \in \mathcal{C}_{T_t}$ , we treat it as previously grounded object and select observation perspectives  $\mathcal{I}_i^*$  following Sec. 4.2, but prioritize maximizing its coverage (detailed in **Appendix**) to focus on the candidate  $c_i$ . The final set of perspectives is the union over all candidates:

$$\mathcal{I}^* = \bigcup_{c_i \in \mathcal{C}_{T_t}} \mathcal{I}_i^*. \quad (9)$$

Once perspectives are determined, we perform annotation to facilitate grounding like existing methods [19, 24, 25, 38, 59]. Prior methods either annotate only candidates, leading VLMs to miss key cues, or annotate all objects in the view, introducing excessive irrelevant content that confuses VLMs. We mark both previously grounded objects and current candidates, and obtain annotated images  $\mathcal{I}_A^*$ : a single annotation per previously localized object, providing VLMs with sufficient cues while avoiding distractions. Full procedure and visualizations are detailed in the **Appendix**.

**VLM Reasoning.** Inspired by prior works [13, 25, 59], we feed the query  $Q$  to the VLM to extract structured semantic conditions for the target label  $L_{T_t}$ . The structured decomposition disentangles the complex linguistic instructions into interpretable criteria, such as spatial relations and attributes, facilitating precise reasoning in the subsequent stage. Next, both annotated  $\mathcal{I}_A^*$  and non-annotated  $\mathcal{I}^*$  are provided to the VLM for multi-view reasoning. In particular, annotated views supply explicit spatial cues of objects, while non-annotated ones preserve holistic visual perception without potential visual occlusion caused by excessive annotations, as observed in SeeGround [24]. Then, the VLM checks which object satisfies all conditions and outputs the grounded object  $O_t$  for task  $T_t$ .

## 5. Experiments

### 5.1. Experimental Settings

**Datasets.** We evaluate OpenGround on three datasets to assess both open-world and  $\mathcal{OLT}$ -dependent grounding performance. For open-world evaluation, we conduct experiments on all 7,724 queries of OpenTarget (details in Sec. 3), which contains part-level objects beyond usual categories to simulate the open-world scenarios, to test the ability to localize open-world objects. For  $\mathcal{OLT}$ -dependent evaluation, we use two popular benchmark datasets: ScanRefer [6] and Nr3D [1]. ScanRefer provides 51,500 descriptions over 800 ScanNet [9] scenes. We follow the standard protocol and report results on its validation set with 9,508 queries. Nr3D, part of the ReferIt3D benchmark [1], includes 41,503 queries collected via a two-player reference game and offers ground-truth 3D bounding boxes for all objects. We evaluate on its validation set with 7,805 queries.

**Implementation Details.** Our experiments utilize the open-source GLM-4.5V [51] as the VLM, CLIP-ViT-Base-Patch16 text encoder [40] for text similarity matching, GroundedSAM [43] as SEG and set  $V=3$ ,  $\tau_{iou}=0.5$ ,  $\tau_{cand}=0.9$  where  $\tau_{iou}, \tau_{cand}$  follow existing works. For the  $\mathcal{OLT}$  on ScanRefer and OpenTarget benchmarks, we follow the object detection procedure outlined in ZSVG3D [64] for consistency in evaluation and fair comparison, which utilizes Mask3D [44] to obtain the predefined  $\mathcal{OLT}$ .

### 5.2. Comparative Study

We conduct comprehensive experiments across multiple benchmarks, including Nr3D [1], ScanRefer [6], and OpenTarget. Detailed performance, on ScanRefer [6] and Nr3D [1], breakdowns across different task categories are presented in Tab. 1 and Tab. 2 with results of competing methods directly from their original publications, while comparisons on OpenTarget are presented in Tab. 3. Due to time constraints, we only evaluate the performance of several recently proposed top-performing and open-source zero-shot methods on OpenTarget, where all methods adopt the same VLM (GLM-4.5V [51]) to ensure a fair comparison.

**Nr3D & ScanRefer.** Our method achieves competitive zero-shot performance across both benchmarks. On Nr3D [1], we use GPT-4o [37] (consistent with SPAZER [19]) and achieve 61.7% accuracy which is comparable to the zero-shot SOTA SPAZER. Notably, SPAZER relies on advanced candidate selection and pre-filtering strategies that yield significant gains in the “Easy” category, which is discussed in **Appendix**. On ScanRefer [6], our method attains 61.8% (Acc@0.25) and 53.1% (Acc@0.50), outperforming all existing zero-shot baselines. Notably, our results substantially narrow the performance gap with supervised methods.

**OpenTarget.** On the open-world benchmark, existing methods are constrained by Mask3D’s [44] predefined

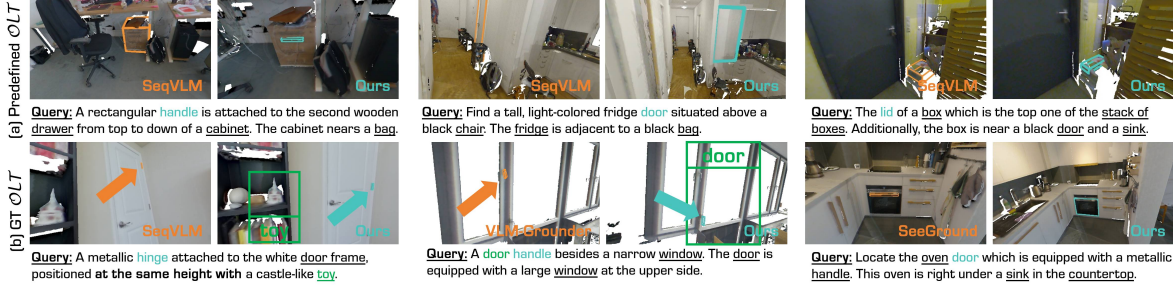


Figure 6. Qualitative Comparisons on **OpenTarget**. (a) compares our method with previous open-source SoTA method, SeqVLM [25] with predefined  $\mathcal{OLT}$ . They fail to ground objects out-of- $\mathcal{OLT}$ . (b) compares our method with previous methods equipped with ground-truth  $\mathcal{OLT}$ . these baselines either overlook key objects (e.g., toy, door) or are distracted by numerous relevant objects, leading to failures.

Table 1. Quantitative Comparisons on **ScanRefer** [6]. Results are reported for “Unique” (scenes with a single target object) and “Multiple” (scenes with distractors of the same class) subsets, with metrics Acc@0.25 and Acc@0.50. \* denotes results on selected 250 samples.

Method	Supervision	VLM	Unique		Multiple		Overall	
			Acc@0.25	Acc@0.50	Acc@0.25	Acc@0.50	Acc@0.25	Acc@0.50
ScanRefer [6]	Supervised	-	67.6	46.2	32.1	21.3	39.0	26.1
ViewSRD [13]	Supervised	-	82.1	68.2	37.4	29.0	45.4	36.0
3D-R1 [15]	Supervised	-	-	-	-	-	<b>65.8</b>	<b>59.2</b>
GPT4Scene [38]	Supervised	-	90.3	83.7	56.4	50.9	62.6	57.0
TSP3D [10]	Supervised	-	-	-	-	-	56.4	46.7
SeeGround [24]	Zero-Shot	Qwen2-VL-72b [55]	75.7	68.9	34.0	30.0	44.1	39.4
SeqVLM [25]	Zero-Shot	Doubaoo-1.5-pro [5]	77.3	72.7	47.8	41.3	55.6	49.6
VLM-Grounder* [59]	Zero-Shot	GPT-4o [37]	51.6	32.8	<b>66.0</b>	29.8	48.3	33.5
SPAZER [19]	Zero-Shot	GPT-4o [37]	<b>80.9</b>	72.3	51.7	43.4	<b>57.2</b>	48.8
ZSVG3D [64]	Zero-Shot	GPT-4 turbo [37]	63.8	58.4	27.7	24.6	36.4	32.7
<b>Ours</b>	Zero-Shot	GLM-4.5V [51]	<b>77.8</b>	<b>74.4</b>	<b>57.9</b>	<b>47.9</b>	<b>61.8</b>	<b>53.1</b>

Table 2. Detailed Performance on **Nr3D** [1]. Queries are categorized as “Easy” (with one distractor) or “Hard” (with multiple distractors), and as “Dep.” (View-Dependent) or “Indep.” (View-Independent) based on viewpoint requirements for grounding.

Method	Easy	Hard	Dep.	Indep.	Overall
3D-R1 [15]	-	-	-	-	68.8
TSP3D [10]	-	-	-	-	48.7
ViewSRD [13]	75.3	64.8	68.6	70.6	69.9
VLM-Grounder [59]	55.2	39.5	45.8	49.4	48.0
SeeGround [24]	54.5	38.3	42.3	48.2	46.1
ZSVG3D [64]	46.5	31.7	36.8	40.0	39.0
SeqVLM [25]	58.1	47.4	51.0	54.5	53.2
SPAZER [19]	<b>68.0</b>	<b>58.8</b>	<b>59.9</b>	<b>66.2</b>	<b>63.8</b>
<b>Ours</b>	<b>64.3</b>	<b>59.3</b>	<b>59.2</b>	<b>63.1</b>	<b>61.7</b>

$\mathcal{OLT}$  which lacks the target objects for grounding, resulting in severely degraded performance (visualized in Fig. 6(a)). To fairly assess their upper bound, we further evaluate them with ground-truth (GT)  $\mathcal{OLT}$ . However, they are still confounded by the proliferation of relevant objects and exponentially larger candidate pool (discussed in the **Appendix**), resulting in erroneous predictions and the underperforming results visualized in Fig. 6(b).

Table 3. Performance on **OpenTarget**. \* denotes results on randomly selected 300 samples due to its low efficiency

Method	$\mathcal{OLT}$	Acc@0.25	Acc@0.50
SeeGround [24]	GT	17.9	17.4
VLM-Grounder* [59]	-	12.3	9.6
VLM-Grounder* [59]	GT	<u>28.6</u>	<u>20.4</u>
SeqVLM [25]	GT	19.4	19.2
GPT4Scene [38]	GT	12.1	11.8
<b>Ours</b>	Mask3D [44] +ACE	<b>46.2</b>	<b>34.2</b>

and reported in Tab. 3. In contrast, our approach achieves 46.2%/34.2%(Acc@0.25/Acc@0.50), far surpassing zero-shot baselines although they are given GT  $\mathcal{OLT}$ . This validates that our ACR module effectively extends the  $\mathcal{OLT}$  to perceive novel objects, enabling open-world grounding.

### 5.3. Ablation Study

To comprehensively validate each module in OpenGround, we conduct extensive ablation studies on the OpenTarget dataset. All experiments use the same settings as the main results, and we report Acc@0.50.

**Effect of Predefined  $\mathcal{OLT}$ .** As shown in Tab. 4, rows

Table 4. Ablation study on different components in our framework on OpenTarget Acc@0.50. **Initial  $\mathcal{OLT}$** : whether using initial object lookup table from Mask3D [44]; **Task Chain**: strategy for constructing task chain; **Relevant Annotation**: annotation method in single-step grounding; **VLM**: the vision-language model used.

#	Initial $\mathcal{OLT}$	Task Chain	Relevant Annotation	VLM	Acc
(1)	Yes	Full	Yes	GLM-4.5V [51]	34.2
(2)	No	Full	Yes	GLM-4.5V [51]	27.1
(3)	Yes	Jump	Yes	GLM-4.5V [51]	29.8
(4)	Yes	Relevance	Yes	GLM-4.5V [51]	32.6
(5)	Yes	Difficulty	Yes	GLM-4.5V [51]	31.5
(6)	Yes	Random	Yes	GLM-4.5V [51]	29.2
(7)	Yes	Full	No(Candidates)	GLM-4.5V [51]	28.8
(8)	Yes	Full	No(All Objects)	GLM-4.5V [51]	20.3
(9)	Yes	Full	Yes	Qwen3-VL-32B [49]	30.4
(10)	Yes	Full	Yes	Qwen3-VL-235B [49]	32.8
(11)	Yes	Full	Yes	Step3 [50]	33.4

Locate a slender wooden **handle** attached to a white **drawer** in a kitchen **cabinet** unit beneath a smooth **countertop** and beside a black **oven**. The handle is situated between other two handles. The cabinet rests against a dark **backsplash**, with a wall-mounted **rack** nearby.



Figure 7. **Task Chain Construction Strategy Results Comparison.** The orange mask area is the objects skipped by the jump strategy. **Jump** strategy incorrectly identifies the object (orange) because it skips the key object, rack. **Full** strategy correctly identifies the object (teal), considering the rack (purple).

(1) and (2), OpenGround remains effective even without a predefined  $\mathcal{OLT}$ , outperforming baselines that use ground-truth  $\mathcal{OLT}$ . Nevertheless, incorporating an initial  $\mathcal{OLT}$  offers a beneficial prior that further improves performance.

**Task Chain Construction Strategy.** We compare several strategies in Sec. 4.1 for constructing the cognitive task chain. As shown in Tab. 4 (rows 1, 3-6), our full strategy performs the best, leaving a large margin. Fig. 7 illustrates a comparison between **Jump** and **Full** strategies, where the latter exhibits more coherent reasoning and accurate localization through progressive cognitive planning. Considering both Tab. 4 and Fig. 4b, we find that strategies more human-like yield superior grounding performance, emphasizing the value of our constructed human-like task chain in open-world grounding.

**Annotation Design in Single-Step Grounding.** Previous methods either annotate all objects in a view, causing visual

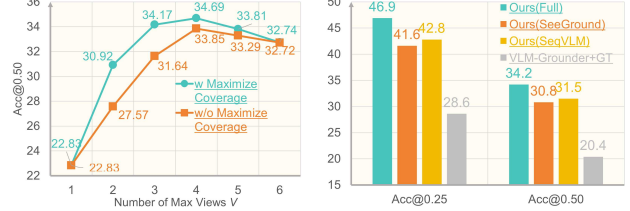


Figure 8. Ablation Study: (a) evaluates the impact of different perspective selection strategies with varying numbers of max views  $V$ ; (b) compares different single-step grounding backbones, where ‘VLM-Grounder+GT’ in (b) corresponds to the Acc@0.50 of VLM-Grounder [59] with GT  $\mathcal{OLT}$  in the Tab. 3.

clutter, or only the candidates, losing useful spatial context. We propose a balanced strategy that annotates both previously grounded objects and current candidates. As shown in Tab. 4, rows (1), (7) and (8), our design effectively preserves visual clarity while providing contextual cues.

**Influence of VLM.** To verify VLM dependence and resource adaptability, we replace the default GLM-4.5V [51] with VLMs of varying scales. As shown in Rows (1) and (9)-(11) of Tab. 4, switching to smaller VLMs induces minimal performance degradation, even that the compact Qwen3-VL-32B [49] only drops 3.8% in Acc@0.50. This confirms our framework’s core advantage stems from the ACR module rather than large-scale VLM capabilities: notably, the 32B small model still outperforms baselines that leverage GT  $\mathcal{OLT}$  (e.g., 10% higher than VLM-Grounder).

**Perspectives Selection Strategy.** As illustrated in Fig. 8, we further study the impact of the view-selection strategy:

- **Number of views  $V$ :** We analyze the impact of  $V$  on performance. When  $V = 1$ , both strategies start at the same low baseline. As  $V$  increases to 4, performance of both strategies rises significantly: ‘w Maximize Coverage’ strategy peaks at 34.7, and ‘w/o Maximize Coverage’ peaks at 33.8. Exceeding  $V = 4$  leads to performance drops, indicating that excessive views introduce redundancy and confusion. Though  $V = 4$  is most accurate, it only brings a 0.52% gain over  $V = 3$  but increases input views by 33.3%. We adopt  $V = 3$  in our experiments for a balance of performance and efficiency.
- **Maximizing Coverage Strategy:** The ‘w Maximize Coverage’ strategy (teal line) consistently outperforms ‘w/o Maximize Coverage’ (orange line) across all  $V$  values. This demonstrates that maximizing object coverage in perspective selection avoids the ACE module missing critical visual information, resulting in higher accuracy.

**Compatibility with Other Methods.** We evaluate the compatibility of our framework with existing grounding approaches. As shown in Fig. 8(b), the single-step grounding module can be seamlessly replaced with prior methods such as SeeGround [24] and SeqVLM [25] without modi-

fication. Results show that our ACE module enables their open-world grounding ability and our cognitive task chain boosts performance, confirming that OpenGround is a general and flexible paradigm rather than a standalone method.

**Limitation.** Our method is designed for static scenes and assumes spatially proximal relevant objects, which are common constraints in current 3D visual grounding. Additionally, ACE’s performance depends on the segmentation model, which lies beyond the scope of our research which focuses on cognition-based reasoning for open-world grounding. These aspects are left for future exploration. More details can be found in **Appendix**.

## 6. Conclusion

This paper presents OpenGround, a novel framework for zero-shot open-world 3D visual grounding. To overcome the limitation of existing methods that rely on a predefined object lookup table ( $\mathcal{OLT}$ ), OpenGround introduces an Active Cognition-based Reasoning (ACR) mechanism. ACR mimics human-like active perception by first structuring a Cognitive Task Chain to leverage contextual relationships, and then employing an Active Cognitive Enhancement module to dynamically expand the object lookup table ( $\mathcal{OLT}$ ) for richer scene understanding. To evaluate our method on open-world scenarios, we also contribute the OpenTarget benchmark. Extensive experiments show that OpenGround remains competitive on standard datasets (Nr3D, SceneRefer) and achieves state-of-the-art performance on OpenTarget, demonstrating its flexibility and superior capability in open-world scenarios.

# OpenGround: Active Cognition-based Reasoning for Open-World 3D Visual Grounding

## Supplementary Material

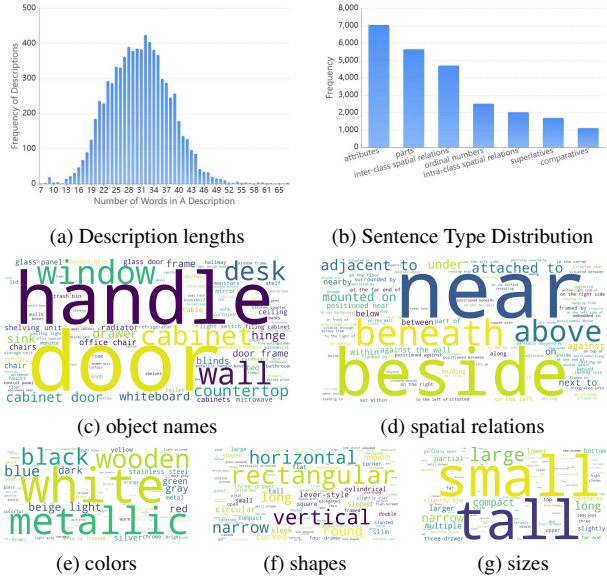


Figure 9. **Dataset Statistics.** (a) shows the word count distribution, indicating balanced conciseness. (b) shows the frequency of sentence categories including attributes (fundamental object properties), parts (object components), intra-class spatial relations (same-category object positions), inter-class spatial relations (different-category object positions), ordinal numbers (sequential order), superlatives (extreme degrees), and comparatives (comparisons), showing syntactic diversity. (c)-(g) are Word clouds of terms for the OpenTarget dataset. Bigger fonts indicate more frequent terms in the descriptions.

## 7. Dataset Details

### 7.1. Dataset Construction Details

We adopt *Qwen3-VL-235B-A22B-Instruct* [49], with 1.2 temperature and prompt in Tab. 9, to generate annotations. In multiple VLMs verification, we utilize *Qwen3-VL-235B-A22B-Instruct* [49], *Qwen3-VL-235B-A22B-Thinking* [49], *Qwen2.5-VL-72B-Instruct* [3], *GLM-4.5V* [51], *Step3* [50] and *Deepseek-VL2* [58], with same settings that temperature is 0.2 and prompt is illustrated in Tab. 10.

### 7.2. Dataset Statistics

We analyze the OpenTarget dataset’s core characteristics in Fig. 9, including 7,724 valid descriptions with word counts ranging 7-72. As shown in Fig. 9a, the length distribution is roughly normal (mode: 32 words, 5.49%), with over 98.1% of descriptions exceeding 16 words, ensuring comprehen-

sive detail. Fig. 9b categorizes descriptions into 7 compatible sentence types (a single description can belong to multiple types, so counts sum to more than 7,724, as illustrated in Tab. 5). Three dominant categories emerge: ‘attributes’ (7,039, 91.13%) is fundamental and easily combined with other categories; ‘parts’ (5,642, 73.04%) is driven by the dataset’s part-level focus; ‘inter-class spatial relations’ (4,705, 60.91%) is inflated by part-parent object descriptions. Remaining types (intra-class spatial relations, ordinals, superlatives, comparatives) ensure syntactic diversity. Word clouds (Figs. 9c to 9g) demonstrate notable lexical richness: as illustrated, vocabulary related to object names, spatial relations, colors, shapes, and sizes is all diverse and abundant, enabling precise and varied descriptive expressions.

## 8. Method Details

### 8.1. Supplementary for Task Chain Construction

In the main paper, we compute a **Weighted Average Edit Distance (WAED)**, to evaluate how closely a model-generated task chain aligns with human cognitive ordering. All computations follow the formulation below.

**Levenshtein Edit Distance.** Given two sequences  $\mathbf{a}$  and  $\mathbf{b}$ , the Levenshtein edit distance  $ED(\mathbf{a}, \mathbf{b})$  is defined as the minimum number of edit operations required to transform  $\mathbf{a}$  into  $\mathbf{b}$ , where the allowed operations are: insertion of one element, deletion of one element and substitution of one element.

**Model-to-Human WAED.** For each task instance  $t$ , the human questionnaire yields a set of sequences  $\{\mathbf{h}_{t,i}\}$  with corresponding frequencies (weights)  $w_{t,i}$ . For a model prediction  $\mathbf{s}_t$ , the weighted average edit distance is:

$$WAED(\mathbf{s}_t) = \frac{\sum_i w_{t,i} ED(\mathbf{s}_t, \mathbf{h}_{t,i})}{\sum_i w_{t,i}}. \quad (10)$$

Averaging across all sequences gives the final reported score:

$$WAED_{\text{model}} = \frac{1}{T} \sum_{t=1}^T WAED(\mathbf{s}_t). \quad (11)$$

**Human–Human Internal Inconsistency.** Within each task instance  $t$ , humans produce multiple valid orderings. We measure their internal disagreement by computing the pairwise weighted edit distance:

Table 5. **Sentence Type Examples.** Attributes: (1-6); parts: (2-6); comparatives: (3), (5); superlatives: (4); inter-class spatial relations: (1-6); intra-class spatial relations: (3), (6); ordinal numbers: (6).

(1)	It is a small black rectangular panel mounted on a vertical pipe beside a white door.
(2)	It is the lid of a small black rectangular panel mounted on a vertical pipe beside a white door.
(3)	It is a metallic hinge, the upper one, mounted on a white door frame. The door features a metallic handle and a closing mechanism at the top, positioned near a ladder and storage items.
(4)	It is a small, round metallic knob mounted on the rightmost door of a tall, light-wood cabinet with four doors. The cabinet stands against the wall near a blue door, beneath exposed ceiling ductwork.
(5)	A metallic hinge attached to the white door frame, positioned at the same height with a castle-like toy.
(6)	Locate the silver handle on the second drawer from the top of a white four-drawer cabinet. The cabinet sits beside a blue office chair, under a small desk with an open cardboard box, near a floral couch.

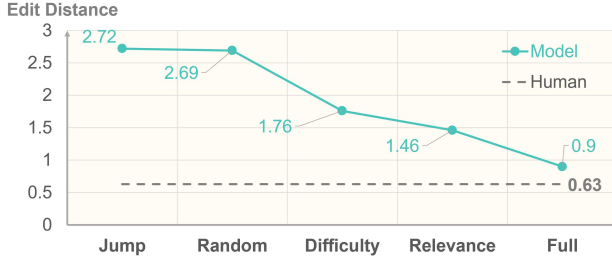


Figure 10. Edit Distances with Human Inconsistency.

$$\text{WAED}_t^{\text{human}} = \sum_{i < j} \left( \frac{w_{t,i} w_{t,j}}{(\sum_k w_{t,k})^2} \right) \text{ED}(\mathbf{h}_{t,i}, \mathbf{h}_{t,j}). \quad (12)$$

Finally, the overall human–human inconsistency level is:

$$\text{WAED}_{\text{human}} = \frac{\sum_t ((\sum_k w_{t,k}) \text{WAED}_t^{\text{human}})}{\sum_t \sum_k w_{t,k}}. \quad (13)$$

This is the internal inconsistency level between human annotators and serves as the reference baseline in Fig. 10.

## 8.2. Cognitive Representation in ACE

We emphasize that the core contribution of the Active Cognition Enhancement (ACE) module lies in the idea of cognitive enhancement, meaning the process of actively refining scene understanding to resolve ambiguity. This idea is not tied to any specific data format. The realization of cognition is flexible and can be built on different forms of scene representations, such as the Cognitive Map used in ThinkInSpace [62] or other voxel-based memory designs. In this work, we adopt the object lookup table ( $\mathcal{OLT}$ ) as the concrete form of scene cognition. This choice ensures compatibility with widely used zero-shot 3DVG pipelines and allows fair comparisons across all evaluated methods.

## 8.3. Perspective Selection in ACE

We show the pseudo code of Sec. 4.2 in Algorithm 1, including fallback strategy for non previously grounded objects provided. The fallback strategy iteratively samples views whose observations contribute sufficiently new, non-overlapping 3D points to the accumulated global scene coverage. Each candidate view is evaluated by the proportion of newly observed points, and only views exceeding a minimal coverage threshold are retained. This ensures efficient scene exploration while avoiding redundant observations.

## 8.4. Perspective Selection in Single-Step Grounding

As illustrated in Algorithm 2, our single-step grounding module selects observation views for each candidate object by prioritizing its own visibility while still maximizing the coverage of previously grounded objects. For every candidate view, we compute two types of gains: a primary gain that measures how many new points of the current candidate object become observable, and a secondary gain that measures the additional coverage contributed to all previously grounded objects. We then perform a lexicographic selection controlled by a soft margin  $\alpha$ : a view is preferred if it yields a strictly higher primary gain, or if its primary gain is within an  $\alpha$ -fraction of the best value while providing a higher secondary gain. After selecting a view, both the candidate’s observed region and the observed regions of all previously grounded objects are updated. The algorithm iteratively selects views until reaching the view budget or until both the candidate object and all previously grounded objects become fully observed.

## 8.5. Annotation in Single-Step Grounding

As a supplementary explanation, Tab. 4 (rows 1 and 7-8) illustrates the impact of different annotation methods, revealing substantial performance differences. Here, as illustrated in Fig. 11, we provide a qualitative visualization of representative samples to intuitively demonstrate how these annotation strategies lead to noticeably different results. As shown in Fig. 11, our proposed annotation strategy effec-

**Algorithm 1** Perspective Selection in ACE

```

Require: Previously grounded objects  $O = \{O_1, \dots, O_{t-1}\}$ , point clouds  $\mathcal{P}$ , max views  $V$ , all RGB images  $\mathcal{I}$ 
1: Initialize observed regions  $\mathcal{R}_{O_i} \leftarrow \emptyset$  for all  $O_i$ 
2:  $\mathcal{I}^* \leftarrow \emptyset$ 
3: for  $v = 1$  to  $V$  do
4:    $\Delta^* \leftarrow 0$ ,  $k^* \leftarrow \text{None}$ 
5:   for each candidate view  $k \notin \mathcal{I}^*$  do
6:      $\Delta \leftarrow 0$ 
7:     for each object  $O_i$  do
8:        $new\_pts \leftarrow (\mathcal{P}_{O_i} \cap \mathcal{P}_k) \setminus \mathcal{R}_{O_i}$ 
9:        $\Delta \leftarrow \Delta + |new\_pts| / |\mathcal{P}_{O_i}|$ 
10:    end for
11:    if  $\Delta > \Delta^*$  then
12:       $\Delta^* \leftarrow \Delta$ 
13:       $k^* \leftarrow k$ 
14:    end if
15:  end for
16:  if  $k^* = \text{None}$  then
17:    break
18:  end if
19:   $\mathcal{I}^* \leftarrow \mathcal{I}^* \cup \{\mathbf{I}_{k^*}\}$ 
20:  for each object  $O_i$  do
21:     $\mathcal{R}_{O_i} \leftarrow \mathcal{R}_{O_i} \cup (\mathcal{P}_{O_i} \cap \mathcal{P}_{k^*})$ 
22:  end for
23:  if  $\forall O_i, \mathcal{R}_{O_i} = \mathcal{P}_{O_i}$  then
24:    break
25:  end if
26: end for
27: if  $\mathcal{I}^* = \emptyset$  then       $\triangleright$  Fallback strategy: observe whole scene
28:    $\mathcal{OP} \leftarrow \emptyset$ 
29:   Define threshold  $\tau$ 
30:   for each candidate view  $k$  do
31:      $new\_pts \leftarrow \mathcal{P}_k \setminus \mathcal{OP}$ 
32:     if  $\frac{|new\_pts|}{|\mathcal{P}_k|} < \tau$  then
33:       continue
34:     end if
35:      $\mathcal{I}^* \leftarrow \mathcal{I}^* \cup \{\mathbf{I}_k\}$ 
36:      $\mathcal{OP} \leftarrow \mathcal{OP} \cup \mathcal{P}_k$ 
37:   end for
38: end if
39: return  $\mathcal{I}^*$ 

```

tively balances informativeness and distraction, leading to more accurate and robust grounding.

- **All Objects Mentioned.** It annotates all query-relevant objects introduces excessive distractions (*e.g.*, irrelevant “object” which is green in Fig. 11b), overwhelming the VLM with irrelevant regions.
- **All Candidates.** It annotates only candidates, missing

**Algorithm 2** Perspective Selection in Single-Step Grounding

**Require:** Candidate object  $c_j$ , previously grounded objects  $O = \{O_1, \dots, O_{t-1}\}$ , point clouds  $\mathcal{P}$ , max views  $V$ , all RGB images  $\mathcal{I}$

- 1: Define soft margin  $\alpha$
- 2: Initialize observed regions  $\mathcal{R}_{O_i} \leftarrow \emptyset$  for all  $O_i$
- 3:  $\mathcal{R}_{c_j} \leftarrow \emptyset, \mathcal{I}_j^* \leftarrow \emptyset$
- 4: **for**  $v = 1$  to  $V$  **do**
- 5:      $k^* \leftarrow \text{None}$
- 6:      $\Delta_p^* \leftarrow 0$  ▷ Primary Gain
- 7:      $\Delta_s^* \leftarrow 0$  ▷ Secondary Gain
- 8:     **for** candidate view  $k \notin \mathcal{I}_j^*$  **do**
- 9:          $new\_c\_pts \leftarrow (\mathcal{P}_{c_j} \cap \mathcal{P}_k) \setminus \mathcal{R}_{c_j}$
- 10:          $\Delta_p \leftarrow |new\_c\_pts| / |\mathcal{P}_{c_j}|$
- 11:          $\Delta_s \leftarrow 0$
- 12:         **for** each object  $O_i$  **do**
- 13:              $new\_prev\_pts \leftarrow (\mathcal{P}_{O_i} \cap \mathcal{P}_k) \setminus \mathcal{R}_{O_i}$
- 14:              $\Delta_s \leftarrow \Delta_s + |new\_prev\_pts| / |\mathcal{P}_{O_i}|$
- 15:         **end for**
- 16:         **if**  $\Delta_p > \Delta_p^*$  or  $(\Delta_p > \alpha \Delta_p^* \text{ and } \Delta_s > \Delta_s^*)$  **then**
- 17:              $\Delta_p^* \leftarrow \max(\Delta_p, \Delta_p^*)$
- 18:              $\Delta_s^* \leftarrow \Delta_s$
- 19:              $k^* \leftarrow k$
- 20:         **end if**
- 21:     **end for**
- 22:     **if**  $k^*$  is None or  $\Delta_s \simeq 0$  **then**
- 23:         **break**
- 24:     **end if**
- 25:      $\mathcal{I}_j^* \leftarrow \mathcal{I}_j^* \cup \{I_{k^*}\}$
- 26:      $\mathcal{R}_{c_j} \leftarrow \mathcal{R}_{c_j} \cup (\mathcal{P}_{O_i} \cap \mathcal{P}_{k^*})$
- 27:     **for** each object  $O_i$  **do**
- 28:          $\mathcal{R}_{O_i} \leftarrow \mathcal{R}_{O_i} \cup (\mathcal{P}_{O_i} \cap \mathcal{P}_{k^*})$
- 29:     **end for**
- 30:     **if**  $\mathcal{R}_{c_j} = \mathcal{P}_{c_j}$  and  $\forall O_i, \mathcal{R}_{O_i} = \mathcal{P}_{O_i}$  **then**
- 31:         **break**
- 32:     **end if**
- 33: **end for**
- 34: **return**  $\mathcal{I}_j^*$

critical spatial context from previously grounded objects (e.g., “the machine-like object marked with ‘Ultimaker’” which is only visible when close enough).

- **Ours.** Our method marks previously grounded objects and current candidates. Since previously grounded objects are definitively localized, each contributes exactly a single annotation (e.g., “object:78” and “cabinet:126”). This avoids the distraction from previously grounded objects in strategy (b) while preserving critical context from grounded objects, which strategy (c) fails to provide.

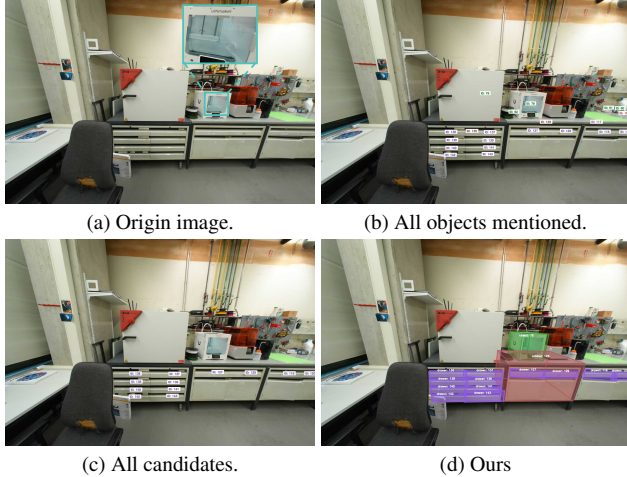


Figure 11. **Annotation Visualization.** The query is “*Locate the drawer directly beneath the machine-like object marked with ‘Ulti-maker’. The drawer is a part of the cabinet under the machine-like object.*” (a) is the origin image without any annotations. (b) annotates all objects mentioned (“drawer”, “cabinet”, “object”) in the query. (c) only annotates all candidates for “drawer”. (d) annotates previously grounded objects and all candidates.

## 9. Implementation Details

For the GroundedSAM [43], we utilize Swin-B GroundingDINO Decoder [30] with text and box thresholds both set to 0.4, and utilize ViT-H SAM2 [41] to generate instance masks from the bounding boxes generated by GroundingDINO, which is also applied to VLM-Grounder [59] on OpenTarget.

### 9.1. Details of Prompt Designs

We adopts different prompts for different tasks of the VLM. We conduct prompt example in Tab. 11 for **Objects Parsing** in Sec. 4.1, Tab. 12 for **Task Chain Construction** in Sec. 4.1, Tab. 13 for conditions extraction in **VLM Reasoning**, and Tab. 14 for reasoning in Sec. 4.3.

### 9.2. Details of Compared Methods

For a fair and rigorous comparison, we reproduce recently top-performing and open-source baselines on OpenTarget under a unified evaluation protocol, using same VLM (GLM-4.5V [51]) for methods requiring VLM. Below we describe our reproduction pipeline and the adaptations necessary to run each method on our benchmark.

**SeeGround [24] + GT.** Since SeeGround is designed to consume ScanRefer-style inputs, we reorganize our OpenTarget annotations into the ScanRefer format. The ground-truth  $\mathcal{OLT}$  (object lookup table) is treated as the predicted object proposals required by SeeGround, enabling it to bypass its default grounding step. All other components of the pipeline strictly follow the official implementation.

Table 6. Performance on **OpenTarget**. \* denotes results on randomly selected 300 samples due to its low efficiency

Method	$\mathcal{OLT}$	Acc@0.25	Acc@0.50
SeeGround [24]	GT	17.9	17.4
VLM-Grounder* [59]	GT	28.6	20.4
SeqVLM [25]	GT	19.4	19.2
GPT4Scene [38]	GT	12.1	11.8
<b>Ours</b>	Mask3D [44] +ACE	<u>46.2</u>	<u>34.2</u>
<b>Ours</b>	GT	<b>54.8</b>	<b>54.3</b>

**SeqVLM [25] + GT.** We feed the ground-truth  $\mathcal{OLT}$  as its  $\mathcal{OPT}$ . Following the settings in the original paper, we generate a multi-view sequence with ( $n_{\text{frame}} = 5$ ) for each candidate object, and we apply the same VLM-based reasoning procedure with a chain length of ( $L = 4$ ) in official implementation. The remainder of the pipeline, including the iterative reasoning logic, remains unchanged.

**VLM-Grounder [59].** To reproduce VLM-Grounder on our dataset, we uniformly sample the image sequence with a ratio of 20:1, consistent with the original paper. We adopt all hyperparameter settings as reported. Due to computational considerations, we use GroundingDINO [30] instead of GroundingDINO-v1.5 [42] as the 2D detector.

**VLM-Grounder [59] + GT.** We further evaluate an oracle variant of VLM-Grounder using ground-truth object information. Building upon the setup above, we replace the View Pre-selection stage with ground-truth projections obtained from  $\mathcal{OLT}$  to directly generate instance masks. We disable the OV-Detection module and instead use the ground-truth  $\mathcal{OLT}$  entries whose categories match the target class. The final Multi-View Ensemble Projection step is replaced by directly selecting the most relevant ground-truth bounding box from  $\mathcal{OLT}$ . The above adaption fully assess the upper bound of VLM-Grounder through fully leveraging the ground-truth  $\mathcal{OLT}$ .

**GPT4Scene [38] + GT.** For GPT4Scene, we use their released finetuned model. Following the original pipeline, we uniformly sample 64 images and render one ceiling-free top-down BEV map from the point cloud. We annotate these images using the ground-truth  $\mathcal{OLT}$ . The reasoning procedure then strictly follows the official prompts described in the paper.

## 10. Additional Quantitative Results

### 10.1. Effect of Large Candidate Pool

As discussed in the main paper, the large candidate pool introduced by the ground-truth  $\mathcal{OLT}$  can mislead existing single-step grounding methods. Without the ACE module, these baselines must directly operate on all GT candidates, many of which are irrelevant, causing increased am-

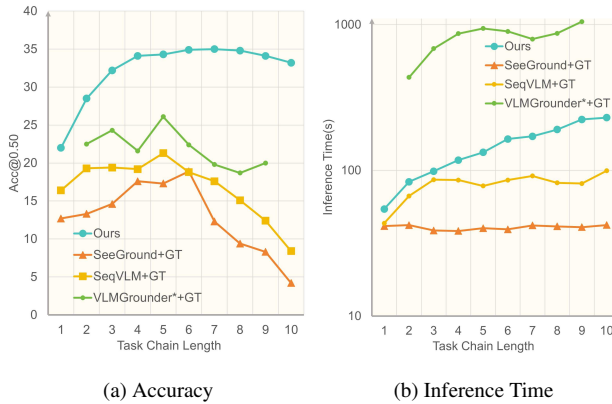


Figure 12. **Comparison across Task Chain Length.** “VLMGrounder\*+GT” is evaluated only on a subset of 300 samples (due to its extremely high computational cost) and lacks values at  $L = 1$  and  $L = 10$  because such chain lengths do not appear in the sampled subset.

biguity and consistent performance degradation. For fairness, we also evaluate our method under the same setting by replacing our initial  $\mathcal{OLT}$  with the full GT  $\mathcal{OLT}$ . Results in Tab. 6 show that our method remains robust and even achieves better performance in this large-pool scenario. This is because our cognitive planning and progressive grounding mechanisms effectively filter out distractors and leverage the additional valid candidates from GT  $\mathcal{OLT}$ .

## 10.2. Comparison across Task Chain Length

To further analyze the effect of cognitive task chain, we compare accuracy and computational cost on OpenTarget. The results are summarized in Fig. 12.

**Accuracy on Task Chain Length.** As illustrated in Fig. 12a, our method keeps high accuracy across all chain lengths which means different difficulties in common scenarios. Notably, the performance advantage is most pronounced for long chains ( $L = 8 - 10$ ) where both “SeeGround [24]+GT” and “SeqVLM [25]+GT” show a consistent performance drop at larger chain lengths, which demonstrates that our cognitive planning and progressive grounding provide the strong benefit.

**Inference Time on Task Chain Length.** As shown in Fig. 12b, the inference time of our method grows gradually with the task chain length, which is expected because deeper cognitive chains invoke more reasoning steps and require processing a larger set of intermediate observations. Importantly, the increase is smooth and well-behaved: the curve follows a near-linear trend on the logarithmic scale, indicating that our progressive reasoning introduces a controlled and predictable computational cost rather than an exponential overhead. In contrast, “SeeGround [24]+GT” and “SeqVLM [25]+GT” maintain relatively flat time curves

since they do not perform multi-step reasoning. However, their lower computational cost comes at the expense of significantly reduced accuracy on longer chains, highlighting the trade-off between shallow reasoning and robust grounding. “VLMGrounder\* [59]+GT” exhibits a substantially higher runtime. Its runtime should also be interpreted with caution: due to the extremely large volume of VLM API calls required by VLM-Grounder, the method frequently exceeds the provider’s tokens-per-minute (TPM) limits, resulting in additional waiting time. Moreover, its values at  $L = 1$  and  $L = 10$  are missing because such chain lengths do not appear in the sampled subset. This extremely high computational cost makes VLM-Grounder impractical for large-scale or long-chain scenarios.

## 10.3. Results on Different Segmentation Models

Since GroundedSAM [43] is one of the most widely adopted and general-purpose open-vocabulary 2D segmentation frameworks, we conduct our 2D-based comparisons by varying only the underlying SAM model size (e.g., ViT-B/L/H), while keeping all other components of our pipeline unchanged. This allows us to isolate the effect of segmentation quality on the downstream grounding performance and ensures that improvements are not confounded by differences in detection or reasoning modules. In addition to the 2D setting, we also evaluate our method with open-vocabulary 3D segmentation model. For this variant, we replace the original **2D Segmentation and Lifting** stage with a **3D Segmentation and Filtering** procedure. Specifically, we directly segment instances in 3D space and then filter out objects that are not visible under the selected views, ensuring consistency with the view-dependent grounding pipeline. Results in Tab. 8 demonstrate that while stronger SAM variants improve performance in 2D-based settings, incorporating open-vocabulary 3D segmentation also provides an competitive results.

## 10.4. Advanced Candidate Selection Strategy

In the main paper, we observe that SPAZER [19] performs much better in the “easy” category on Nr3D [1], leading to its overall advantage on the benchmark. Although the method is not open-sourced, we conjecture that its gain stems from an aggressive candidate selection strategy that removes the single distractor typically present in this split, greatly simplifying the search space. To test whether this heuristic also benefits our pipeline, we integrate SPAZER’s candidate selection module into our framework. As illustrated in Tab. 7, the improvement on Nr3D [1] is marginal. Notably, this experiment highlights the compatibility and extensibility of our approach: our framework can seamlessly incorporate external candidate selection techniques, while maintaining strong performance.

Table 7. Detailed Performance on Nr3D [1]. “+” means that the method is equipped with the candidate selection strategy in SPAZER [19], which is fully compatible with our framework and can be seamlessly integrated. Queries are categorized as “Easy” (with one distractor) or “Hard” (with multiple distractors), and as “Dep.” (View-Dependent) or “Indep.” (View-Independent) based on viewpoint requirements for grounding. Results on GLM-4.5V [51] are also listed here for reference.

Method	VLM	Easy	Hard	Dep.	Indep.	Overall
SPAZER [19]	GPT-4o [37]	68.0	58.8	59.9	66.2	63.8
<b>Ours</b>	GPT-4o [37]	64.3	59.3	59.2	63.1	61.7
<b>Ours<sup>+</sup></b>	GPT-4o [37]	<b>70.1</b>	<b>59.8</b>	<b>60.4</b>	<b>67.2</b>	<b>64.8</b>
<b>Ours</b>	GLM-4.5V [51]	59.1	54.7	54.1	58.3	56.8
<b>Ours<sup>+</sup></b>	GLM-4.5V [51]	64.8	55.2	55.6	62.1	59.8

Table 8. Comparison on different segmentation backbones.

Larger SAM variants yield stronger 2D performance, and integrating open-vocabulary 3D segmentation offers competitive results.

Model	Type	Acc@0.50
SAM-B	2D	26.7
SAM-L	2D	31.5
SAM-H(Ours)	2D	<b>34.2</b>
Open3DIS [36]	3D	<u>33.6</u>

## 11. Potential Solution for Limitation

Our main paper focuses on the conceptual framework of open-world grounding, several practical extensions can mitigate the limitations discussed in the main paper. The following extensions primarily strengthen system robustness or engineering completeness. In contrast, our main paper emphasizes the conceptual advances: open-world grounding formulation and the OpenTarget benchmark. Therefore, we discuss these in the Appendix for completeness.

**Static-Scene Assumption.** While the static-scene assumption is fundamental to existing 3D visual grounding benchmarks, several directions could relax it in future extensions. One potential solution is to move from a single reconstructed scene to a 4D (spatio-temporal) representation, using RGB-D video with scene flow or object tracking to enable grounding within short, locally static time windows. Another approach is static–dynamic decomposition, where dynamic SLAM or motion segmentation separates stable background geometry from moving objects, allowing OpenGround to operate on the static component while handling dynamic objects through small local reconstructions. Alternatively, a tracking-then-grounding paradigm can ground objects in a near-static frame and maintain their positions over time via 2D or 3D tracking. These directions are promising but introduce substantial engineering complexity beyond the conceptual scope of our open-world grounding framework, so we leave them as future work.

**Spatial-Proximity Assumption.** For references that are spatially far apart, global reasoning can be introduced with-

out requiring full exploration. During reasoning, a BEV (bird’s-eye-view) layout can assist long-range spatial inference, while in ACE, a BEV-based spatial partition could guide the VLM to first select plausible regions before performing detailed observation and cognition enhancement.

**Dependence on Segmentation Quality.** Segmentation robustness can be improved using ensemble segmentation. It combines predictions from multiple segmentation models (e.g., different SAM variants or architectures), allowing the system to aggregate consensus regions and suppress model-specific errors. This typically reduces fragmentation and improves mask stability across diverse environments.

**Error Propagation in Task Chain.** Because later grounding depends on earlier steps, an incorrect early prediction may propagate through the task chain. A lightweight engineering extension can mitigate this: during Single-Step Grounding, if the VLM detects that no candidate satisfies all conditions, it can backtrack to the previous step, discard the inconsistent hypothesis, and re-ground the object before continuing. This provides a practical safeguard against rare cascading errors without altering the core framework, whereas non-progressive grounding methods cannot benefit from such corrective backtracking.

## 12. More Visualization Results

We provide additional qualitative results to further illustrate the behavior of OpenGround in both benchmark and real-world open-world settings. Fig. 13 presents comparisons on the OpenTarget benchmark, where we show ground-truth views, our predictions, and SeqVLM+GT. Correct and incorrect predictions are highlighted, and key linguistic cues are underlined to reveal how the model reasons over queries. Beyond benchmark evaluation, Fig. 14 demonstrates OpenGround applied to ScanNet++, where target objects even fall outside OpenTarget categories. These examples highlight OpenGround’s ability to generalize to truly open-world objects and perform reliable localization even in cluttered, unseen environments. In addition, we further evaluate our method in fully open-world outdoor scenes where non  $\mathcal{OLT}$  provided, as shown in Fig. 15.

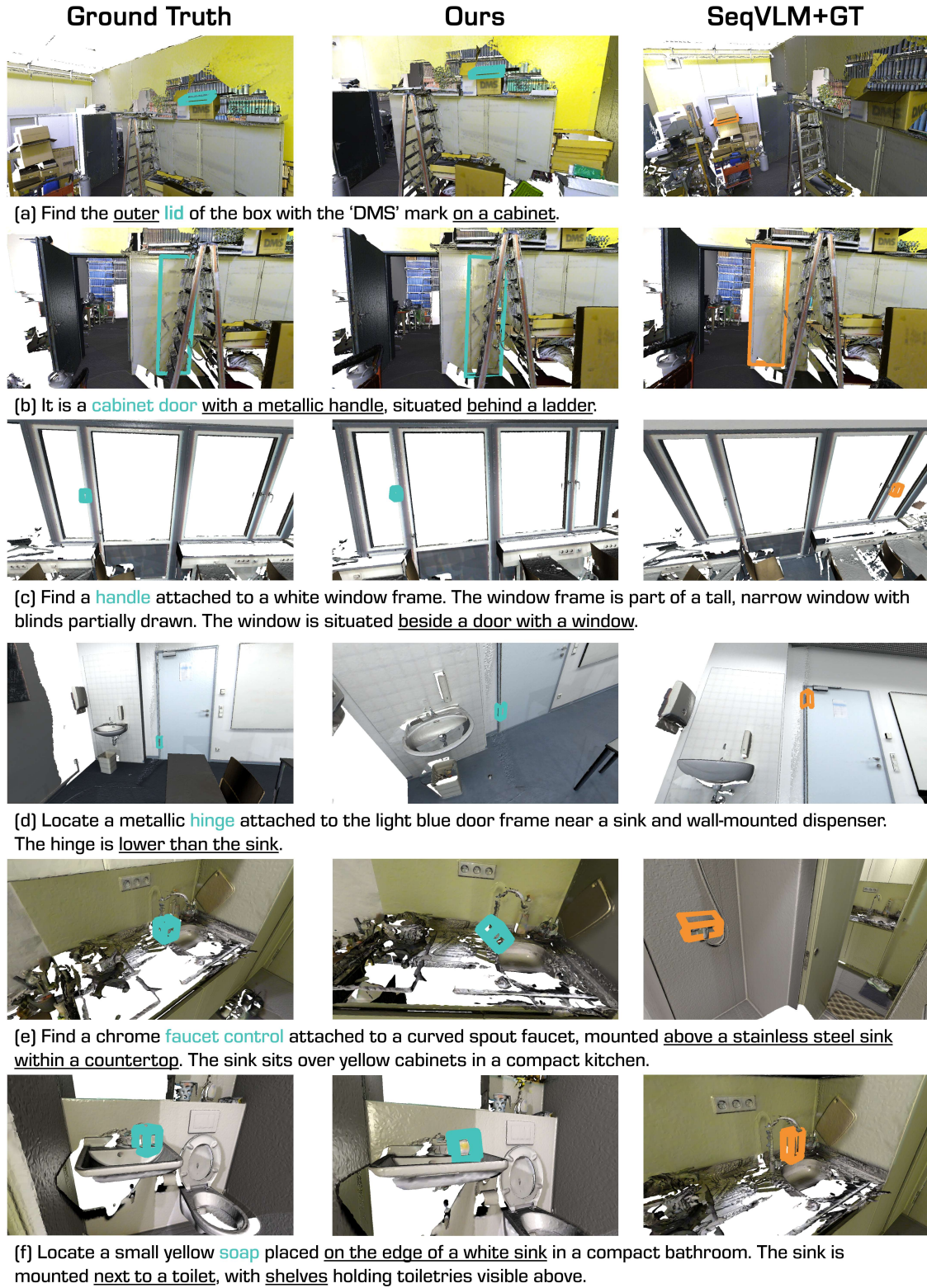


Figure 13. **Visualization of OpenGround on the OpenTarget benchmark.** Correct predictions are shown in teal and incorrect predictions in orange. Key linguistic cues used for grounding are underlined.

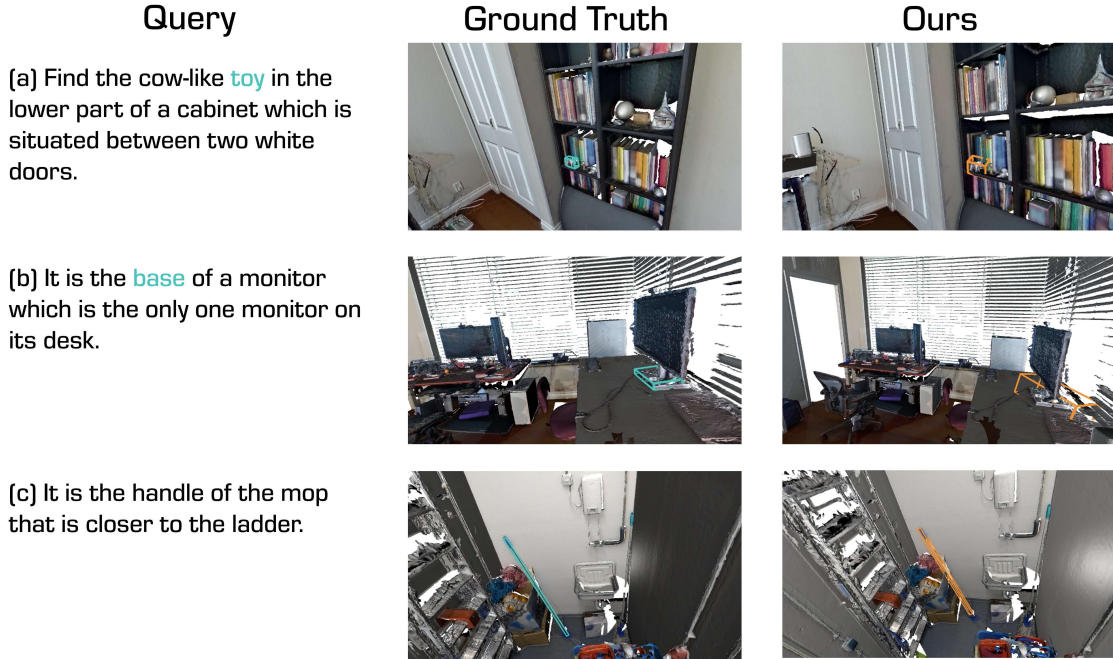


Figure 14. **Visualization of OpenGround on Application in ScanNet++ [63].** The target object (Ground Truth) is even out of OpenTarget, actually open-world object.

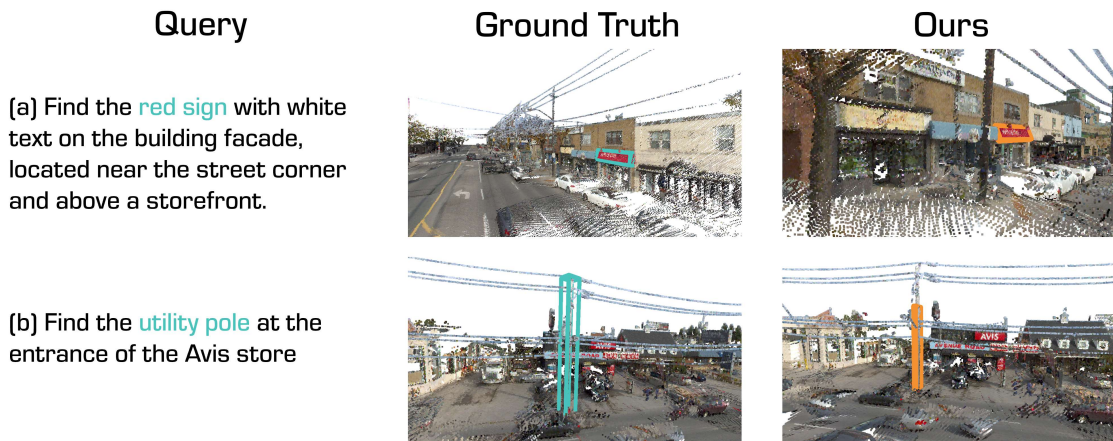


Figure 15. **Visualization of OpenGround on Application in Toronto3D [48].** The target object (Ground Truth) is also out of predefined categories in Toronto3D, actually open-world object.

Table 9. Prompt for dataset annotation. “{images}” represents the input images, “{label hierarchy}” is the label hierarchy of the target object, and “{context reference}” is the generated annotation of the parent of the target object.

<b>Prompt Template for Dataset Annotation</b>
Please analyze user’s input images, label hierarchy and context reference. Label hierarchy consists of current object label and its parent objects’ labels. Context reference is the description of current object’s direct parent. $\langle \text{image\_1} \rangle$ is the image observing the target object, and $\langle \text{image\_2} \rangle \dots \langle \text{image\_N} \rangle$ are the images observing distractors with same label. All objects in images are marked with red bounding boxes. Your task is generate a discriminative description for the object in the bounding box of $\langle \text{image\_1} \rangle$ . The description should distinguish the object from distractors and keep information from context reference. Attention: 1. Words ‘bounding box’ and ‘image’ should not appear in your answer. 2. It would be better to figure out the target object explicitly as example does. 3. It would be better to vary sentence structure, compared to the context reference and the examples. <b>Here are examples:</b> Example 1: Images: $\langle \text{image\_1} \rangle, \langle \text{image\_2} \rangle, \langle \text{image\_3} \rangle, \langle \text{image\_4} \rangle$ Label hierarchy: “cabinet” $\rightarrow$ “drawer” $\rightarrow$ “handle”. Context reference: “Find a wooden drawer which is the second from top to down of a cabinet. The cabinet nears a backpack.” Output: Locate a rectangular handle is attached to the second wooden drawer from top to down of a cabinet. The cabinet nears a backpack. Example 2: Images: $\langle \text{image\_1} \rangle, \langle \text{image\_2} \rangle$ Label hierarchy: “door”. Context reference: None Output: Locate a wooden door which is near a whiteboard. ... <b>Now, start your task:</b> Images: {images}. Label hierarchy: {label hierarchy}. Context reference: {context reference}.

Table 10. Prompt for dataset verification. “{images}” represents the input images and “{query}” is the generated annotation of the target object.

### Prompt Template for Dataset Verification

Please analyze user’s input images and query. Your task is reasoning on query and determine the image whose object in the red bounding box satisfies the query. Return the result strictly in this JSON format without any addition content:

```
{  
  "answer": {  
    "reason": "xxx",  
    "image": xxx  
  }  
}
```

#### Here are example:

Example 1:

Images: <image\_1>, <image\_2>, <image\_3>, <image\_4>

Query: Locate a rectangular handle is attached to the second wooden drawer from top to down of a cabinet. The cabinet nears a backpack.

Response:

```
{  
  "answer": {  
    "reason": "<image_1> ... <image_4> are handles on the same cabinet.  
    <image_1> is the second from top, <image_2> is the third from top,  
    <image_4> is the forth from top, and <image_4> is the first top one.  
    So the answer is <image_1> ",  
    "image": 1  
  }  
}
```

...

#### Now, start your task:

Image: {images}. Query: {query}.

Table 11. Prompt for parsing relevant and target objects from the query description. “{query}” represents the input query  $Q$ .

### Prompt Template for Objects Parsing

Please analyze the user’s input query and identify all specific physical objects mentioned in it (exclude abstract concepts, actions, areas, or standalone attributes). Explicitly relevant objects should also be considered. Return the result strictly in this JSON format without any additional content:

```
{
  "objects": [
    {"name": "object1", "is_target": true/false},
    {"name": "object2", "is_target": true/false}
  ]
}
```

Only one object may be marked as target (is\_target=true). All other objects must be marked as non-target (is\_target=false).

**Here are examples:**

Example 1:

Query: “Locate the box which is the top one of the stack of boxes on the floor. Additionally, the box is near a black door and a sink in a storage room.”

Response:

```
{
  "objects": [
    {"name": "box", "is_target": true},
    {"name": "boxes stack", "is_target": false},
    {"name": "door", "is_target": false},
    {"name": "sink", "is_target": false}
  ]
}
```

Example 2:

Query: “A small metallic hinge attached to the door frame at the lower part”

Response:

```
{
  "objects": [
    {"name": "hinge", "is_target": true},
    {"name": "door frame", "is_target": false},
    {"name": "door", "is_target": false} % relevant to door frame
  ]
}
```

...

**Now, start your task:**

Query: {query}.

Table 12. Prompt for constructing cognitive task chain. “{query}” represents the input query  $\mathcal{Q}$ , “{relevant objects}” represents the list of relevant objects and their candidate counts, and “{target}” represents the target object and its candidate count.

### Prompt Template for Cognitive Task Chain Construction

Please analyze the user’s input query, related objects and corresponding candidates counts. Your task is sorting it into a sequence which follows human manner and considers both semantic relevance and difficulty (including both candidates counts and visibility), for a robot to ground it in a room. Return the result strictly in the following JSON format without any additional content:

```
{
  "reason": "xxx",
  "sequence": [
    { "name": "object2", "origin_index": 1},
    { "name": "object1", "origin_index": 0},
    { "name": "object3", "origin_index": -1} // It is the target object
  ]
}
```

The target object should always be placed at last.

#### Here are examples:

Example 1:

Query: “Locate the box which is the top one of the stack of boxes on the floor. Additionally, the box is near a black door and a sink in a storage room.”

Relevant Objects: [ (“boxes stack”, 0), (“door”, 3), (“sink”, 2)]

Target Object: (“box”, 17)

Response:

```
{
  "reason": "Sink (2 candidates) is most salient fixture in storage rooms...",
  "sequence": [
    { "name": "sink", "origin_index": 2},
    ...
    { "name": "box", "origin_index": -1}
  ]
}
```

Example 2:

Query: “Locate a slender wooden handle attached to a white drawer in a kitchen cabinet unit beneath a smooth countertop and beside a black oven. The handle is situated between other two handles. The cabinet rests against a dark backslash, with a wall-mounted rack nearby.”

Relevant Objects: [ (“oven”, 1), (“countertop”, 1), (“cabinet”, 10), (“rack”, 0), (“backslash”, 0), (“drawer”, 0)]

Target Object: (“handle”, 0) Response:

```
{
  "reason": "Oven (1 candidate) and countertop (1 candidate) are highly...",
  "sequence": [
    { "name": "oven", "origin_index": 0},
    ...
    { "name": "handle", "origin_index": -1}
  ]
}

...
```

#### Now, start your task:

Query: {query}. Relevant Objects: {relevant objects}. Target Object: {target}.

Table 13. Prompt for conditions retrieval. “{query}” represents the input query  $Q$ , “{related objects}” represents the objects in the task chain, and “{target}” represents the object to retrieve conditions in this step.

### Prompt Template for Conditions Retrieval

Please analyze the user’s input query, related objects and the target object. Your task is summarize the conditions of the target object. Return the result strictly in the following JSON format without any additional content:

```
{  
    "conditions": [  
        "condition1", "condition2", ...  
    ]  
}
```

The output conditions should be detailed and sufficient.

#### Here are examples:

Example 1:

Query: “Locate the box which is the top one of the stack of boxes on the floor. Additionally, the box is near a black door and a sink in a storage room.”

Related Objects: [“sink”, ..., “box”]

Target Object: “boxes stack”

Response:

```
{  
    "conditions": [  
        "it is a stack of boxes",  
        "it is on the floor",  
        "it is near a black door",  
        "it is near a sink"  
    ]  
}
```

...

#### Now, start your task:

Query: {query}. Related Objects: {related objects}. Target Object: {target}.

Table 14. Prompt for VLM reasoning. “{images}” represents the combined image set with annotate images  $\mathcal{I}_A^*$  and non-annotated images  $\mathcal{I}^*$ , “{query}” represents the input query  $\mathcal{Q}$ , and “{conditions}” represents the conditions obtained in Tab. 13.

### Prompt Template for VLM Reasoning

Please analyze user’s input query, the conditions of the target object and images. For each N,  $\langle \text{image\_}2N-1 \rangle$  is origin image without any annotation,  $\langle \text{image\_}2N \rangle$  is the annotated images with previously grounded objects (which might be appeared in the conditions) and current candidates. Each annotation is consists of a bounding box, a label and corresponding id. Your task is matching each candidate with the conditions. Return the result strictly in the following JSON format without any additional content:

```
{
  "id1": ["condition1", "condition3"],
  "id2": ["condition2"],
  ...
}
```

You should observe and compare the images carefully. The output conditions should be exactly the same as the input.

#### Here are examples:

Example 1:

Images:  $\langle \text{image\_}1 \rangle$ ,  $\langle \text{image\_}2 \rangle$ ,  $\langle \text{image\_}3 \rangle$ ,  $\langle \text{image\_}4 \rangle$

Query: “Locate the box which is the top one of the stack of boxes on the floor. Additionally, the box is near a black door and a sink in a storage room.”

Conditions: [ “it is a stack of boxes”, “it is on the floor”, “it is near a black door”, “it is near a sink” ]

Response:

```
{
  "128": ["it is a stack of boxes", "it is on the floor"],
  "127": ["it is a stack of boxes"],
  ...
  "131": [
    "it is a stack of boxes",
    "it is on the floor",
    "it is near a black door",
    "it is near a sink"
  ]
}

...
```

#### Now, start your task:

Images: {images}. Query: {query}. Conditions: {conditions}.

## References

[1] Panos Achlioptas, Ahmed Abdelreheem, Fei Xia, Mohamed Elhoseiny, and Leonidas Guibas. Referit3d: Neural listeners for fine-grained 3d object identification in real-world scenes. In *European conference on computer vision*, pages 422–440. Springer, 2020. [1](#) [2](#) [3](#) [5](#) [6](#) [7](#)

[2] Jinze Bai, Shuai Bai, Shusheng Yang, Shijie Wang, Sinan Tan, Peng Wang, Junyang Lin, Chang Zhou, and Jingren Zhou. Qwen-vl: A versatile vision-language model for understanding, localization, text reading, and beyond. [arXiv](#)

[3] Shuai Bai, Keqin Chen, Xuejing Liu, Jialin Wang, Wenbin Ge, Sibo Song, Kai Dang, Peng Wang, Shijie Wang, Jun Tang, Humen Zhong, Yuanzhi Zhu, Mingkun Yang, Zhao-hai Li, Jianqiang Wan, Pengfei Wang, Wei Ding, Zheren Fu, Yiheng Xu, Jiabo Ye, Xi Zhang, Tianbao Xie, Zesen Cheng, Hang Zhang, Zhibo Yang, Haiyang Xu, and Junyang Lin. Qwen2.5-vl technical report. [arXiv preprint arXiv:2308.12966](#), 2023. [2](#)

[4] Gilad Baruch, Zhuoyuan Chen, Afshin Dehghan, Tal Dimry, Yuri Feigin, Peter Fu, Thomas Gebauer, Brandon Joffe, Daniel Kurz, Arik Schwartz, et al. Arkitscenes: A diverse real-world dataset for 3d indoor scene understanding using mobile rgb-d data. [arXiv preprint arXiv:2111.08897](#), 2021. [1](#)

[5] ByteDance. Volcengine, 2025. Accessed: 2025-02-18. [7](#)

[6] Dave Zhenyu Chen, Angel X Chang, and Matthias Nießner. Scanrefer: 3d object localization in rgb-d scans using natural language. In *European conference on computer vision*, pages 202–221. Springer, 2020. [1](#) [2](#) [3](#) [6](#) [7](#)

[7] Runnan Chen, Youquan Liu, Lingdong Kong, Xinge Zhu, Yuexin Ma, Yikang Li, Yuenan Hou, Yu Qiao, and Wenping Wang. Clip2scene: Towards label-efficient 3d scene understanding by clip. In *Proceedings of the IEEE/CVF Conference on Computer Vision and Pattern Recognition*, pages 7020–7030, 2023. [1](#)

[8] Zhe Chen, Jiannan Wu, Wenhui Wang, Weijie Su, Guo Chen, Sen Xing, Muyan Zhong, Qinglong Zhang, Xizhou Zhu, Lewei Lu, et al. Internvl: Scaling up vision foundation models and aligning for generic visual-linguistic tasks. In *Proceedings of the IEEE/CVF Conference on Computer Vision and Pattern Recognition*, pages 24185–24198, 2024. [2](#)

[9] Angela Dai, Angel X Chang, Manolis Savva, Maciej Halber, Thomas Funkhouser, and Matthias Nießner. Scannet: Richly-annotated 3d reconstructions of indoor scenes. In *Proceedings of the IEEE conference on computer vision and pattern recognition*, pages 5828–5839, 2017. [1](#) [6](#)

[10] Wenxuan Guo, Xiuwei Xu, Ziwei Wang, Jianjiang Feng, Jie Zhou, and Jiwen Lu. Text-guided sparse voxel pruning for efficient 3d visual grounding. In *Proceedings of the Computer Vision and Pattern Recognition Conference*, pages 3666–3675, 2025. [1](#) [2](#) [7](#)

[11] Anna-Maria Halacheva, Yang Miao, Jan-Nico Zaech, Xi Wang, Luc Van Gool, and Danda Pani Paudel. Holistic understanding of 3d scenes as universal scene description. [arXiv preprint arXiv:2412.01398](#), 2024. [2](#) [3](#)

[12] Chenguang Huang, Oier Mees, Andy Zeng, and Wolfram Burgard. Visual language maps for robot navigation. [arXiv preprint arXiv:2210.05714](#), 2022. [1](#)

[13] Ronggang Huang, Haoxin Yang, Yan Cai, Xuemiao Xu, Huaidong Zhang, and Shengfeng He. Viewsrd: 3d visual grounding via structured multi-view decomposition. In *Proceedings of the IEEE/CVF International Conference on Computer Vision*, pages 9726–9736, 2025. [1](#) [2](#) [6](#) [7](#)

[14] Shihua Huang, Yongjie Hou, Longfei Liu, Xuanlong Yu, and Xi Shen. Real-time object detection meets dinov3. [arXiv](#), 2025. [3](#)

[15] Ting Huang, Zeyu Zhang, and Hao Tang. 3d-r1: Enhancing reasoning in 3d vlm for unified scene understanding. *arXiv preprint arXiv:2507.23478*, 2025. 1, 2, 7

[16] Zanming Huang, Zhongkai Shangguan, Jimuyang Zhang, Gilad Bar, Matthew Boyd, and Eshed Ohn-Bar. Assister: Assistive navigation via conditional instruction generation. In *European Conference on Computer Vision*, pages 271–289. Springer, 2022. 1

[17] Ayush Jain, Nikolaos Gkanatsios, Ishita Mediratta, and Katerina Fragkiadaki. Bottom up top down detection transformers for language grounding in images and point clouds. In *European Conference on Computer Vision*, pages 417–433. Springer, 2022. 2

[18] Li Jiang, Hengshuang Zhao, Shaoshuai Shi, Shu Liu, Chi-Wing Fu, and Jiaya Jia. Pointgroup: Dual-set point grouping for 3d instance segmentation. In *Proceedings of the IEEE/CVF conference on computer vision and Pattern recognition*, pages 4867–4876, 2020. 2

[19] Zhao Jin, Rong-Cheng Tu, Jingyi Liao, Wenhao Sun, Xiao Luo, Shunyu Liu, and Dacheng Tao. Spazer: Spatial-semantic progressive reasoning agent for zero-shot 3d visual grounding, 2025. 2, 6, 7, 5

[20] Alexander Kirillov, Eric Mintun, Nikhila Ravi, Hanzi Mao, Chloe Rolland, Laura Gustafson, Tete Xiao, Spencer Whitehead, Alexander C. Berg, Wan-Yen Lo, Piotr Dollár, and Ross Girshick. Segment anything. *arXiv:2304.02643*, 2023. 3

[21] Lingdong Kong, Youquan Liu, Xin Li, Runnan Chen, Wen-wei Zhang, Jiawei Ren, Liang Pan, Kai Chen, and Ziwei Liu. Robo3d: Towards robust and reliable 3d perception against corruptions. In *Proceedings of the IEEE/CVF International Conference on Computer Vision*, pages 19994–20006, 2023. 1

[22] VI Lcvenshtcin. Binary coors capable or ‘correcting deletions, insertions, and reversals. In *Soviet physics-doklady*, 1966. 5

[23] Jinpeng Li, Haiping Wang, Yuan Liu, Zhiyang Dou, Yuexin Ma, Sibei Yang, Yuan Li, Wenping Wang, Zhen Dong, Bisheng Yang, et al. Cityanchor: City-scale 3d visual grounding with multi-modality llms. In *The Thirteenth International Conference on Learning Representations*. 1, 2

[24] Rong Li, Shijie Li, Lingdong Kong, Xulei Yang, and Junwei Liang. Seeground: See and ground for zero-shot open-vocabulary 3d visual grounding. In *Proceedings of the IEEE/CVF Conference on Computer Vision and Pattern Recognition (CVPR)*, 2025. 1, 2, 6, 7, 8, 4, 5

[25] Jiawen Lin, Shiran Bian, Yihang Zhu, Wenbin Tan, Yachao Zhang, Yuan Xie, and Yanyun Qu. Seqvilm: Proposal-guided multi-view sequences reasoning via vlm for zero-shot 3d visual grounding. In *Proceedings of the 33rd ACM International Conference on Multimedia*, page 3094–3103, New York, NY, USA, 2025. Association for Computing Machinery. 1, 2, 6, 7, 8, 4, 5

[26] Zijun Lin, Shuting He, Cheston Tan, and Bihan Wen. Groundflow: A plug-in module for temporal reasoning on 3d point cloud sequential grounding. *arXiv preprint arXiv:2506.21188*, 2025. 1, 2

[27] Haotian Liu, Chunyuan Li, Yuheng Li, and Yong Jae Lee. Improved baselines with visual instruction tuning, 2023. 2

[28] Haotian Liu, Chunyuan Li, Qingyang Wu, and Yong Jae Lee. Visual instruction tuning, 2023.

[29] Haotian Liu, Chunyuan Li, Yuheng Li, Bo Li, Yuanhan Zhang, Sheng Shen, and Yong Jae Lee. Llava-next: Improved reasoning, ocr, and world knowledge, 2024. 2

[30] Shilong Liu, Zhaoyang Zeng, Tianhe Ren, Feng Li, Hao Zhang, Jie Yang, Chunyuan Li, Jianwei Yang, Hang Su, Jun Zhu, et al. Grounding dino: Marrying dino with grounded pre-training for open-set object detection. *arXiv preprint arXiv:2303.05499*, 2023. 3, 4

[31] Yang Liu, Weixing Chen, Yongjie Bai, Xiaodan Liang, Guanbin Li, Wen Gao, and Liang Lin. Aligning cyber space with physical world: A comprehensive survey on embodied ai. *IEEE/ASME Transactions on Mechatronics*, 2025. 1

[32] Ze Liu, Zheng Zhang, Yue Cao, Han Hu, and Xin Tong. Group-free 3d object detection via transformers. In *Proceedings of the IEEE/CVF international conference on computer vision*, pages 2949–2958, 2021. 2

[33] Zhenyang Liu, Yikai Wang, Sixiao Zheng, Tongying Pan, Longfei Liang, Yanwei Fu, and Xiangyang Xue. Reasongrounder: Lvlm-guided hierarchical feature splatting for open-vocabulary 3d visual grounding and reasoning. In *CVPR*, pages 3718–3727. Computer Vision Foundation / IEEE, 2025. 1

[34] Teli Ma, Rong Li, and Junwei Liang. An examination of the compositionality of large generative vision-language models. *arXiv preprint arXiv:2308.10509*, 2023. 1

[35] Gonzalo Navarro. A guided tour to approximate string matching. *ACM Comput. Surv.*, 33(1):31–88, 2001. 5

[36] Phuc Nguyen, Tuan Duc Ngo, Evangelos Kalogerakis, Chuang Gan, Anh Tran, Cuong Pham, and Khoi Nguyen. Open3dis: Open-vocabulary 3d instance segmentation with 2d mask guidance. In *Proceedings of the IEEE/CVF conference on computer vision and pattern recognition*, pages 4018–4028, 2024. 5, 6

[37] OpenAI. Gpt-4 technical report, 2024. 2, 6, 7

[38] Zhangyang Qi, Zhixiong Zhang, Ye Fang, Jiaqi Wang, and Hengshuang Zhao. Gpt4scene: Understand 3d scenes from videos with vision-language models. *arXiv preprint arXiv:2501.01428*, 2025. 1, 2, 6, 7, 4

[39] Zhipeng Qian, Yiwei Ma, Zhekai Lin, Jiayi Ji, Xiaowu Zheng, Xiaoshuai Sun, and Rongrong Ji. Multi-branch collaborative learning network for 3d visual grounding. In *European Conference on Computer Vision*, pages 381–398. Springer, 2024. 2

[40] Alec Radford, Jong Wook Kim, Chris Hallacy, Aditya Ramesh, Gabriel Goh, Sandhini Agarwal, Girish Sastry, Amanda Askell, Pamela Mishkin, Jack Clark, Gretchen Krueger, and Ilya Sutskever. Learning transferable visual models from natural language supervision, 2021. 6

[41] Nikhila Ravi, Valentin Gabeur, Yuan-Ting Hu, Ronghang Hu, Chaitanya Ryali, Tengyu Ma, Haitham Khedr, Roman Rädle, Chloe Rolland, Laura Gustafson, Eric Mintun, Junting Pan, Kalyan Vasudev Alwala, Nicolas Carion, Chao-Yuan Wu, Ross Girshick, Piotr Dollár, and Christoph Feicht

enhofer. Sam 2: Segment anything in images and videos. *arXiv preprint arXiv:2408.00714*, 2024. 3, 4

[42] Tianhe Ren, Qing Jiang, Shilong Liu, Zhaoyang Zeng, Wenlong Liu, Han Gao, Hongjie Huang, Zhengyu Ma, Xiaoke Jiang, Yihao Chen, Yuda Xiong, Hao Zhang, Feng Li, Peijun Tang, Kent Yu, and Lei Zhang. Grounding dino 1.5: Advance the "edge" of open-set object detection, 2024. 4

[43] Tianhe Ren, Shilong Liu, Ailing Zeng, Jing Lin, Kun-chang Li, He Cao, Jiayu Chen, Xinyu Huang, Yukang Chen, Feng Yan, Zhaoyang Zeng, Hao Zhang, Feng Li, Jie Yang, Hongyang Li, Qing Jiang, and Lei Zhang. Grounded sam: Assembling open-world models for diverse visual tasks, 2024. 3, 6, 4, 5

[44] Jonas Schult, Francis Engelmann, Alexander Hermans, Or Litany, Siyu Tang, and Bastian Leibe. Mask3d: Mask transformer for 3d semantic instance segmentation. *arXiv preprint arXiv:2210.03105*, 2022. 2, 6, 7, 8, 4

[45] Zhihong Shao, Peiyi Wang, Qihao Zhu, Runxin Xu, Junxiao Song, Mingchuan Zhang, Y.K. Li, Y. Wu, and Daya Guo. Deepseekmath: Pushing the limits of mathematical reasoning in open language models, 2024. 2

[46] Jiaxin Shi, Mingyue Xiang, Hao Sun, Yixuan Huang, and Zhi Weng. Chain of semantics programming in 3d gaussian splatting representation for 3d vision grounding. In *CVPR*, pages 24560–24569. Computer Vision Foundation / IEEE, 2025. 1

[47] Serkan Solmaz, Lode Jorissen, and Vasilios Zogopoulos. Scanverse: An extended reality authoring platform for industrial digital twins. *Procedia CIRP*, 136:624–629, 2025. 1

[48] Weikai Tan, Nannan Qin, Lingfei Ma, Ying Li, Jing Du, Guorong Cai, Ke Yang, and Jonathan Li. Toronto-3D: A large-scale mobile lidar dataset for semantic segmentation of urban roadways. In *Proceedings of the IEEE/CVF Conference on Computer Vision and Pattern Recognition Workshops*, pages 202–203, 2020. 8

[49] Qwen Team. Qwen3 technical report, 2025. 2, 8, 1

[50] StepFun Team. Step-3 is large yet affordable: Model-system co-design for cost-effective decoding, 2025. 8, 1

[51] V Team, Wenyi Hong, Wenmeng Yu, Xiaotao Gu, Guo Wang, Guobing Gan, Haomiao Tang, Jiale Cheng, Ji Qi, Junhui Ji, Lihang Pan, Shuaiqi Duan, Weihan Wang, Yan Wang, Yean Cheng, Zehai He, Zhe Su, Zhen Yang, Ziyang Pan, Aohan Zeng, Baoxu Wang, Bin Chen, Boyan Shi, Changyu Pang, Chenhui Zhang, Da Yin, Fan Yang, Guoqing Chen, Jiazheng Xu, Jiale Zhu, Jiali Chen, Jing Chen, Jin-hao Chen, Jinghao Lin, Jinjiang Wang, Junjie Chen, Leqi Lei, Letian Gong, Leyi Pan, Mingdao Liu, Mingde Xu, Mingzhi Zhang, Qinkai Zheng, Sheng Yang, Shi Zhong, Shiyu Huang, Shuyuan Zhao, Siyan Xue, Shangqin Tu, Shengbiao Meng, Tianshu Zhang, Tianwei Luo, Tianxiang Hao, Tianyu Tong, Wenkai Li, Wei Jia, Xiao Liu, Xiaohan Zhang, Xin Lyu, Xinyue Fan, Xuancheng Huang, Yaling Wang, Yadong Xue, Yanfeng Wang, Yanzi Wang, Yifan An, Yifan Du, Yiming Shi, Yiheng Huang, Yilin Niu, Yuan Wang, Yuanchang Yue, Yuchen Li, Yutao Zhang, Yuting Wang, Yu Wang, Yuxuan Zhang, Zhao Xue, Zhenyu Hou, Zhengxiao Du, Zihan Wang, Peng Zhang, Debing Liu, Bin Xu, Juanzi Li, Minlie Huang, Yuxiao Dong, and Jie Tang. Glm-4.5v and glm-4.1v-thinking: Towards versatile multi-modal reasoning with scalable reinforcement learning, 2025. 2, 6, 7, 8, 1, 4

[52] Ozan Unal, Christos Sakaridis, Suman Saha, and Luc Van Gool. Four ways to improve verbo-visual fusion for dense 3d visual grounding. In *European Conference on Computer Vision*, pages 196–213. Springer, 2024. 2

[53] Ozan Unal, Christos Sakaridis, Suman Saha, and Luc Van Gool. Four ways to improve verbo-visual fusion for dense 3d visual grounding. In *European Conference on Computer Vision (ECCV)*, 2024. 1

[54] Thang Vu, Kookhoi Kim, Tung M Luu, Thanh Nguyen, and Chang D Yoo. Softgroup for 3d instance segmentation on point clouds. In *Proceedings of the IEEE/CVF conference on computer vision and pattern recognition*, pages 2708–2717, 2022. 2

[55] Peng Wang, Shuai Bai, Sinan Tan, Shijie Wang, Zhihao Fan, Jinze Bai, Keqin Chen, Xuejing Liu, Jialin Wang, Wenbin Ge, Yang Fan, Kai Dang, Mengfei Du, Xuancheng Ren, Rui Men, Dayiheng Liu, Chang Zhou, Jingren Zhou, and Junyang Lin. Qwen2-vl: Enhancing vision-language model's perception of the world at any resolution. *arXiv preprint arXiv:2409.12191*, 2024. 2, 7

[56] Weiyun Wang, Zhangwei Gao, Lixin Gu, Hengjun Pu, Long Cui, Xingguang Wei, Zhaoyang Liu, Linglin Jing, Shenglong Ye, Jie Shao, et al. Internvl3.5: Advancing open-source multimodal models in versatility, reasoning, and efficiency. *arXiv preprint arXiv:2508.18265*, 2025. 2

[57] Yuan Wang, Yali Li, and Shengjin Wang. G<sup>^</sup> 3-lq: Marrying hyperbolic alignment with explicit semantic-geometric modeling for 3d visual grounding. In *Proceedings of the IEEE/CVF Conference on Computer Vision and Pattern Recognition*, pages 13917–13926, 2024. 2

[58] Zhiyu Wu, Xiaokang Chen, Zizheng Pan, Xingchao Liu, Wen Liu, Damai Dai, Huazuo Gao, Yiyang Ma, Chengyue Wu, Bingxuan Wang, Zhenda Xie, Yu Wu, Kai Hu, Jiawei Wang, Yaofeng Sun, Yukun Li, Yishi Piao, Kang Guan, Aixin Liu, Xin Xie, Yuxiang You, Kai Dong, Xingkai Yu, Haowei Zhang, Liang Zhao, Yisong Wang, and Chong Ruan. Deepseek-vl2: Mixture-of-experts vision-language models for advanced multimodal understanding, 2024. 1

[59] Runsen Xu, Zhiwei Huang, Tai Wang, Yilun Chen, Jiangmiao Pang, and Dahu Lin. Vlm-grounder: A vlm agent for zero-shot 3d visual grounding. In *CoRL*, 2024. 1, 2, 6, 7, 8, 4, 5

[60] Runsen Xu, Xiaolong Wang, Tai Wang, Yilun Chen, Jiangmiao Pang, and Dahu Lin. Pointllm: Empowering large language models to understand point clouds. In *European Conference on Computer Vision*, pages 131–147. Springer, 2024. 2

[61] Jianing Yang, Xuwei Chen, Shengyi Qian, Nikhil Madaan, Madhavan Iyengar, David F Fouhey, and Joyce Chai. Llm-grounder: Open-vocabulary 3d visual grounding with large language model as an agent. In *2024 IEEE International Conference on Robotics and Automation (ICRA)*, pages 7694–7701. IEEE, 2024. 2

[62] Jihan Yang, Shusheng Yang, Anjali W. Gupta, Rilyn Han, Li Fei-Fei, and Saining Xie. Thinking in Space: How Multi-modal Large Language Models See, Remember and Recall Spaces. *arXiv preprint arXiv:2412.14171*, 2024. 2

[63] Chandan Yeshwanth, Yueh-Cheng Liu, Matthias Nießner, and Angela Dai. Scannet++: A high-fidelity dataset of 3d indoor scenes. In *Proceedings of the International Conference on Computer Vision (ICCV)*, 2023. 2, 3, 8

[64] Zhihao Yuan, Jinke Ren, Chun-Mei Feng, Hengshuang Zhao, Shuguang Cui, and Zhen Li. Visual programming for zero-shot open-vocabulary 3d visual grounding. In *Proceedings of the IEEE/CVF Conference on Computer Vision and Pattern Recognition*, pages 20623–20633, 2024. 2, 6, 7

[65] Nader Zantout, Haochen Zhang, Pujith Kachana, Jinkai Qiu, Ji Zhang, and Wenshan Wang. Sort3d: Spatial object-centric reasoning toolbox for zero-shot 3d grounding using large language models. *CoRR*, abs/2504.18684, 2025. 1, 2

[66] Chenlu Zhan, Yufei Zhang, Gaoang Wang, and Hongwei Wang. Freeq-graph: Free-form querying with semantic consistent scene graph for 3d scene understanding, 2025. 2

[67] Yiming Zhang, ZeMing Gong, and Angel X Chang. Multi3drefer: Grounding text description to multiple 3d objects. In *Proceedings of the IEEE/CVF International Conference on Computer Vision*, pages 15225–15236, 2023. 1, 2

[68] Yumin Zhang, Hongliu Li, Yajun Gao, Haoran Duan, Yawen Huang, and Yefeng Zheng. Prototype correlation matching and class- relation reasoning for few-shot medical image segmentation. *IEEE Transactions on Medical Imaging*, 43(11):4041–4054, 2024. 1

[69] Yue Zhang, Ziqiao Ma, Jialu Li, Yanyuan Qiao, Zun Wang, Joyce Chai, Qi Wu, Mohit Bansal, and Parisa Kordjamshidi. Vision-and-language navigation today and tomorrow: A survey in the era of foundation models. *arXiv preprint arXiv:2407.07035*, 2024. 1

[70] Lichen Zhao, Daigang Cai, Lu Sheng, and Dong Xu. 3dvg-transformer: Relation modeling for visual grounding on point clouds. In *Proceedings of the IEEE/CVF International Conference on Computer Vision*, pages 2928–2937, 2021. 2

[71] Henry Zheng, Hao Shi, Qihang Peng, Yong Xien Chng, Rui Huang, Yepeng Weng, Zhongchao Shi, and Gao Huang. Densegrounding: Improving dense language-vision semantics for ego-centric 3d visual grounding. *arXiv preprint arXiv:2505.04965*, 2025. 1, 2

[72] Yuchen Zhou, Jiayuan Gu, Tung Yen Chiang, Fanbo Xiang, and Hao Su. Point-SAM: Promptable 3d segmentation model for point clouds. In *The Thirteenth International Conference on Learning Representations*, 2025. 2

[73] Chenming Zhu, Tai Wang, Wenwei Zhang, Jiangmiao Pang, and Xihui Liu. Llava-3d: A simple yet effective pathway to empowering lmms with 3d-awareness. *arXiv preprint arXiv:2409.18125*, 2024. 2

[74] Fangrui Zhu, Hanhui Wang, Yiming Xie, Jing Gu, Tianye Ding, Jianwei Yang, and Huaizu Jiang. Struct2d: A perception-guided framework for spatial reasoning in large multimodal models. *CoRR*, abs/2506.04220, 2025. 1, 2

[75] Ziyu Zhu, Xiaojian Ma, Yixin Chen, Zhidong Deng, Siyuan Huang, and Qing Li. 3d-vista: Pre-trained transformer for 3d vision and text alignment. In *Proceedings of the IEEE/CVF International Conference on Computer Vision*, pages 2911–2921, 2023. 2

[76] Ziyu Zhu, Xilin Wang, Yixuan Li, Zhuofan Zhang, Xiaojian Ma, Yixin Chen, Baoxiong Jia, Wei Liang, Qian Yu, Zhidong Deng, et al. Move to understand a 3d scene: Bridging visual grounding and exploration for efficient and versatile embodied navigation. In *Proceedings of the IEEE/CVF International Conference on Computer Vision*, pages 8120–8132, 2025. 1